Regulation of dendrite growth, placement, and patterning in *Drosophila melanogaster* class 4 dendrite arborization neurons

Jiae Lee

A dissertation
submitted in partial fulfillment of the
requirements for the degree of

Doctor of Philosophy

University of Washington
2016

Reading Committee:
Jay Z. Parrish, Chair
David M. Parichy
Linda Wordeman

Program Authorized to Offer Degree:
Department of Biology

University of Washington

ABSTRACT

Regulation of dendrite growth, placement, and patterning in
Drosophila melanogaster class 4 dendrite arborization neurons

Jiae Lee

Chair of the Supervisory Committee:
Jay Z. Parrish, Ph.D.
Department of Biology

The directional flow of information in neurons depends on compartmentalization: dendrites receive inputs whereas axons transmit them. Axons and dendrites likewise contain structurally and functionally distinct subcompartments. Axon/dendrite compartmentalization can be attributed to neuronal polarization, but the developmental origin of subcompartments in axons and dendrites is less well understood. To identify the developmental bases for compartment-specific patterning in dendrites, we screened for mutations that affect discrete dendritic domains in Drosophila sensory neurons. From this screen, we identified mutations that affected distinct aspects of terminal dendrite development with little or no effect on major dendrite patterning.

Mutations in tubulin assembly proteins including Tubulin specific chaperone C showed a phenotype that was preferentially affecting the terminal dendrite placement to be shifted towards the soma via controlling compartmentalization specific growth. We performed a detailed analysis of tubulin dynamics to establish a profile of developmental regulation in tubulin cytoskeleton in subcompartments of the dendritic arbor, and we suggest Tbcc as a local, positive regulator of growth in terminal dendrites.

Mutation of another gene, raw, affected multiple aspects of terminal dendrite patterning, suggesting that Raw might coordinate multiple signaling pathways to shape terminal dendrite growth. Consistent with this notion, Raw localizes to branch-points and promotes dendrite stabilization together with the Tricornered (Trc) kinase via effects on cell adhesion.
Raw independently influences terminal dendrite elongation through a mechanism that involves modulation of the cytoskeleton, and this pathway is likely to involve the RNA-binding protein Argonaute 1 (AGO1), as raw and AGO1 genetically interact to promote terminal dendrite growth but not adhesion. Thus, Raw defines a potential point of convergence in distinct pathways shaping terminal dendrite patterning.

TABLE OF CONTENTS

INTRODUCTION

The morphology of a cell is a critical requirement for carrying out its proper function. Achieving the correct morphology through a complicated series of biological processes in the course of development is a major challenge that every cell has to task. In order to establish a proper pattern of the dendrite so the neuron can collect information from its receptive field effectively, regulation of growth is one of the key features a neuron has to control precisely.

The directional flow of information in the nervous system relies on the compartmentalization of neurons. On a basic level, a neuron has two compartments apart from the soma: dendrites, which receive inputs, and axons, which transmit signals. To meet their respective functions, axons and dendrites have distinct morphological and molecular properties. For example, the microtubule cytoskeleton is organized differently in axons and dendrites, allowing distinct modes of trafficking (Baas, Deitch, Black, & Banker, 1988), (Horton & Ehlers, 2003). Beyond this basic level of compartmentalization, neurons display extreme diversity in axon and dendrite morphology, and both axons and dendrites contain structurally and functionally distinct subdomains (Katsuki, Joshi, Ailani, & Hiromi, 2011; Masland, 2004). Several lines of evidence support the existence of compartments within dendrites. First, some neurons have morphologically distinct dendrites. For example, mammalian olfactory bulb mitral cells extend a tufted primary dendrite radially and structurally and functionally distinct lateral dendrites horizontally (Imamura & Greer, 2009). Likewise, apical/basal dendrites of hippocampal neurons and ipsilateral/contralateral dendrites of motoneurons are morphologically and biophysically distinct. Second, specialized structures are asymmetrically distributed in many dendrites. Notable among these is the dendritic spine, an isolated compartment that is electrically

and biochemically distinct from the rest of the dendrite arbor, and dendritic spines likewise have distinctive microdomains (Chen & Sabatini, 2012) (Yuste, 2013). Many organelles are selectively deployed in dendrites, including a satellite secretory pathway containing endoplasmic reticulum and Golgi outposts; the number and location of these organelles locally influences dendrite growth and dynamics (Aridor, Guzik, Bielli, & Fish, 2004; Gardiol, Racca, & Triller, 1999) (Horton & Ehlers, 2003) (Ye et al., 2007). In highly branched dendrite arbors, for example cerebellar Purkinje neurons and insect sensory neurons, major dendrites and terminal dendrites have distinct cytoskeletal compositions and growth properties (Fujishima, Horie, Mochizuki, & Kengaku, 2012; Jinushi-Nakao et al., 2007). Finally, dendrite arbors often contain functionally distinct domains as well. For example, the proximal-distal compartmentalization of chloride co-transporters underlies directional selectivity in starburst amacrine cells (Gavrikov, Nilson, Dmitriev, Zucker, & Mangel, 2006). Whereas axon/dendrite compartmentalization can be attributed to neuronal polarization, the developmental origin of dendrite subcompartments is less well understood.

Drosophila peripheral nervous system (PNS) class IV dendrite arborization (C4da) neurons have highly branched dendrite arbors consisting of major dendrites emanating radially from the soma and terminal dendrites that fill in the space in the receptive field (Grueber, Jan, & Jan, 2002). Main branches and terminal arbors have distinct growth properties in these neurons, with terminal dendrites exhibiting dynamic growth and containing a cytoskeleton largely devoid of microtubules (Grueber et al., 2002) (Jinushi-Nakao et al., 2007), suggesting that different cellular programs pattern main dendrites and terminal arbors. To identify the developmental bases for compartment-specific patterning in these dendrites, we used a genetic screen to identify mutations that affect distinct dendritic compartments. From this screen, we identified mutants

that selectively affected terminal dendrites, including their placement along the proximal-distal axis and their patterning, suggesting that distance from the soma and branch type (major or terminal dendrite) are two key pieces of positional information in the patterning of terminal dendrites.

Mutations in tubulin assembly proteins including Tubulin specific chaperone C showed a phenotype that was preferentially affecting the terminal dendrite placement shifted towards soma via controlling compartmentalization specific growth, and had minimal effects on axons. Tubulin specific chaperones function together as a tubulin assembly machine, marrying the α- and β-tubulin subunits into a tightly associated heterodimer (Tian & Cowan, 2013). Concerted action of a series of chaperone proteins including five tubulin-specific chaperones (TBCs) termed TBCA–TBCE. We suggest Tbcc as a local, positive regulator of growth in terminal dendrites.

Mutations in raw were unique in that they simultaneously affected multiple aspects of terminal dendrite patterning, suggesting that raw coordinately controls multiple aspects of terminal dendrite growth. Indeed, we found that Raw regulates terminal dendrite adhesion and elongation via distinct pathways, the former involving the Trc kinase and the latter involving cytoskeletal remodeling and the RNA-binding protein AGO1. Thus, Raw appears to be a crucial component of a spatially localized program controlling terminal dendrite patterning.

MATERIAL AND METHODS

Live Imaging

Imaging was as described (Jiang, Soba, Parker, Kim, & Parrish, 2014). For time-lapse analysis, larvae were imaged at the indicated time, recovered to yeasted agar plates with vented lids, aged at 25°C, and imaged again.

FRAP analysis/ Photoconversion

Photoconversion and FRAP assays were conducted on a Leica SP5 with a 40×1.25NA oil objective at 1024×256-pixel resolution. For photoconversion, 8 µm of either a terminal or a major dendrite of a *ppk-gal4/+; UAS-aTubulin-EosFP/+* or *ppk-gal4/+; UAS-EosFP/+* was selected as a region of interest (ROI). The ROI was illuminated for 5 s with a 50-mW 405-nm Diode laser (Leica) at 40% output to photoconvert EosFP and imaged at 10 s and 4h post-conversion with a 500–520-nm bandwidth for photoconversion. Intensity was analyzed using line plots (ImageJ) with eight individual samples. For FRAP assays, ROIs in a *ppk-gal4/+; UAS-aTubulin-GFP/+* or *ppk-gal4/+; UAS-GFP/+* were photobleached for 3 s with a 405-nm laser at 60% power such that 60% of the initial fluorescence intensity was bleached. Baseline fluorescence was measured from five images acquired before bleaching, and fluorescence recovery was measured with 20 scans at 2-s intervals after bleaching. Background fluorescence values were subtracted from measurements of a nearby unbleached dendritic region at each time point. To control for photobleaching and sample movement out of focus, fluorescence intensity was monitored in multiple regions of the arbor outside of the ROI; only samples for which

intensities remained steady in these control regions were included in data analysis. Recovery half-time and the recoverable pool were measured using Leica FRAP Wizard software.

Immunohistochemistry

Larval fillets were dissected/processed as described (Grueber et al., 2002) and stained with: HRP conjugated with Cy2 or Cy3 (1:200; Jackson ImmunoResearch, West Grove, PA), mCD8 (1:100; Life Technologies, Carlsbad, CA), phospho-JNK and anti-lacZ (1:500; Cell Signaling, Boston, MA), anti-Trc-P-T449 (1:500), and secondary antibodies from Jackson ImmunoResearch (1:250).

Phospho-Trc antibody

Antibodies from rabbits immunized with a KLH-conjugated phosphorylated peptide (CKDWVFINY-pT-YKRFE) were affinity purified with bead-conjugated phosphopeptide. Non-phospho-specific antibodies were removed by absorption against a nonphosphorylated version of the antigen (Yenzym, Burlingame, CA).

Surface Staining

Formaldehyde (4%) fixed fillets were washed/stained without detergent to prevent permeabilization. Rhodamine-conjugated secondary antibodies were used for surface staining to ensure that surface-exposed GFP could be differentiated from total GFP.

Cell Culture

S2 cells were grown as described (Rogers & Rogers, 2008), transfected using Effectene (Qiagen, Valencia, CA), and treated with 100nM okadaic acid (Sigma, St. Louis, MO) for 30min before harvesting, where indicated.

Immunoprecipitations

Two days post-transfection, cells were lysed in NP-40 buffer. 1mg of extract was incubated with primary antibodies for 2hr, followed by Protein-G Agarose (Roche, Basel, Switzerland) for 1hr. Beads were washed 5x in lysis buffer and bound proteins were analyzed by SDS-PAGE/Western blotting.

Cell Adhesion Assay

Transfected S2 cells were plated for 1 hour in a 6-well cell culture plate coated with Collagen I, Fibronectin, or Laminin (Life Technologies, Carlsbad, CA). Cells were washed 2x with PBS, cells were counted in four fields of view, washed 3x with PBS, counted as before, and we calculated an adhesion index, the ratio of GFP-positive cells before/after washing.

Cell Fractionation

Transfected S2 cells were lysed in 250mM Sucrose fractionation buffer [250mM Sucrose, 20mM HEPES pH 7.4, 10mM KCl, 1.5mM MgCl2, 1mM EDTA, 1mM EGTA, 1mM DTT, Complete protease inhibitor (Life Technologies, Carlsbad, CA)] with Dounce homogenization. Lysates were fractionated by centrifugation: 720g (nuclear), 10,000g (mitochondria), and 100,000g for membrane (pellet) and cytosolic (soluble) fractions.

Molecular Biology

Raw-short was PCR amplified from cDNA clone GH23250 (*Drosophila* Genomics Resource Center, Bloomington, IN) and cloned into pUAST with N-terminal EGFP derived from pEGFP-

N1 (Clontech, Mountain View, CA). Transgenics services were provided by BestGene (Chino Hills, CA).

Measurements

Measurements were as described (Jiang et al., 2014). Details are available in supplemental methods.

Statistical Analysis

Differences between group means were analyzed via ANOVA with a post hoc Dunnett's test; pairwise comparisons of group means were done with a student's t-test. Binomial tests were used to evaluate whether terminal dynamics differed between control and *raw* mutant neurons (Chapter 2, Fig. 2D). Chi-squared tests were used to evaluate whether presence/absence of GFP-Raw at branch-points influenced terminal dynamics (Chapter 2, Fig. 3C).

RESULTS AND DISCUSSION

CHAPTER 1

Regulation of dendrite patterning by compartmentalized microtubule dynamics and local support of tubulin biogenesis

Growth of drosophila sensory da (dendritic arborization) neurons is accompanied by the expansion of the larval body wall carried out through development. As each body segment grows, the major dendrites reach to the boundary and defines the area of coverage but the majority of dendritic material that fill the dendritic coverage field is constituted by the fine terminal dendrites. Measurement of dendrite growth length in major and terminal dendrites of an identical MARCM clone with 24h time interval revealed the major growth contribution was derived from terminal dendrites (Lee, Peng, Lin, & Parrish, 2015).

In order to discover novel intrinsic factors that are required for terminal dendrite growth, we performed an EMS-induced forward genetic screen and looked for abnormal patterns of terminal dendrite placements in mosaic clones that a gene is specifically mutated in a single da neuron, and observed at the final stage of larval development, 120h AEL (After Egg Laying). Interestingly, there were two category of genes of which their mutants showing a common phenotype; one involved in tubulin biogenesis, such as *Tbcc* (Tubulin Binding Chaperone C) and *Cct4* (Chaperonin containing TCP-1, subunit 4) (Figure 1B-C), and the other related to intracellular transport machinery, such as Rab6 (Figure 1D). The phenotype at the 3rd instar stage of these mutants showed restriction of terminal dendrite growth at the distal area and in contrast exuberant growth at the proximal area. At 120h AEL, fewer terminal branches were located

distally whereas more dendrites were placed exuberantly closer to the cell body, resulting in a dramatic proximal shift in branch distribution (Figure 1E). Mutation resulted in marked reduction in receptive field coverage with reduced number of terminal branches (Figure 1G-H). However, at the early stage of development (48h AEL) these mutants did not show significant difference of branch pattern (Figure 1F), total dendrite length, and total number of terminal branches, from the wild type (Figure 1G-H). This phenotype of proximal shift of terminal branches is similar to the dynein light intermediate chain 2 (dlic2) or kinesin heavy chain (khc) mutants which are disrupting polarized dendrite transport (Satoh et al., 2008). Notably, dynein and kinesin mutants were reported to manifest axonal phenotype, including abnormal thickening and branching into multiple neurites within an axon. This phenotype was also observed in Rab6 mutants, presumably due to their intermutual cellular function. However, this axon phenotype is not observed in *Tbcc* and *Cct4* mutants, which suggests an existence of dendrite specific mechanism to regulate terminal dendrite growth, which is not exclusively known to this point. We further investigated on characterization of *Tbcc* to understand the role of tubulin assembly and supply specifically in terminal dendrite growth control.

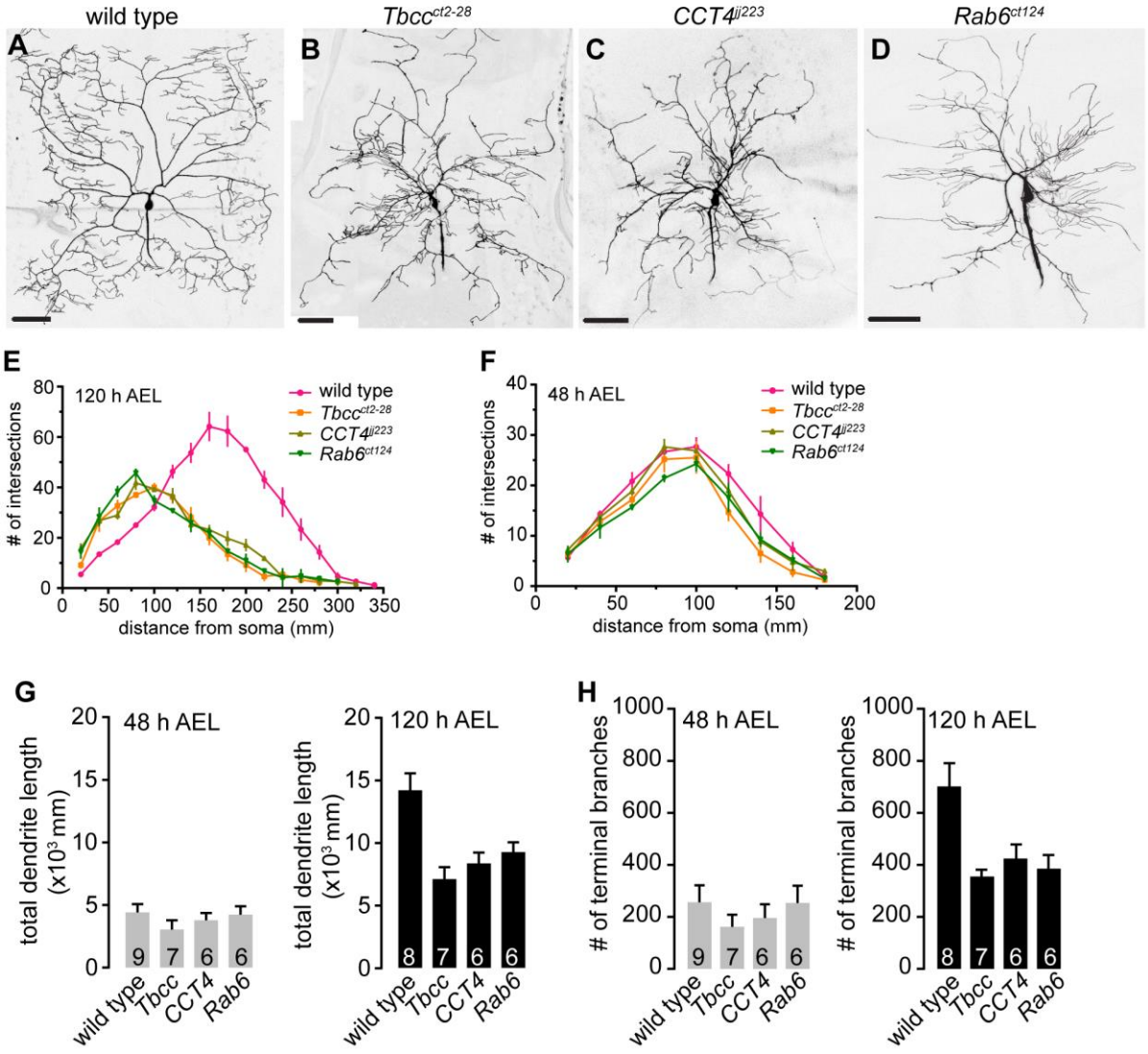

Figure 1. Phenotypic analysis of mutants with terminal branch shift on proximal-distal axis of the dendrite arbor. Representative MARCM clones for wildtype control (A), *Tbcc*$^{ct2\text{-}28}$ (B), *CCT4*^{ij223} (C) and *Rab6*^{ct12} (D). (E-F) Morphometric analysis of dendrites from C4da MARCM clones of the indicated genotypes. Sholl analysis depicting the distribution intersections at 120 AEL (E) and 48h AEL (F) (n=6 for all genotypes). (G-H) Average terminal dendrite length (G) and average number of terminal branches (H) for 48h AEL and 120h AEL; error bars indicate standard deviation.

In order to further evaluate the developmental progress of *Tbcc* phenotype, we created a montage by overlapping two consecutive time lapse camera lucida tracings with 24h interval in respect to the former time point, and pseudo-colored the terminal dendrites that had grown in red, and retracted in blue (Figure 2A). In *Tbcc* mutants, as it develops from 48h to 72h AEL, the distribution of growth is dramatically reversed, both in extent of length and the number of events. Amount of branch growth decreases towards the distal position in *Tbcc*; whereas the amount of retraction is comparable to wild type. This pattern of branch growth dynamics persists as the development advance to 96h AEL and 120h AEL, resulting in sparse terminal branch in the distal region and extensive branching in proximal region of the arbor. Average length of growth in wild type at the distal region is substantially shorter, indicating there are more branch initiation at that region. Again, average length of retraction was comparable in all regions and all time points of *Tbcc* and wild type (Figure 2B). Therefore, we could conclude that the phenotype of *Tbcc* was caused from defect of proper growth of terminal dendrites.

In addition, we wanted to also see if there is a bias of growth in not only the terminal dendrites, but also in the major dendrites. With 50μm distanced bins from the soma, we measured the interstitial length in between identical branch nodes of the major dendrites and compared those lengths in 24 hour developmental intervals. At early developmental stages (48h-72h AEL), there was an increment of major dendrite growth in distal regions, whereas at later stages of development (96h-120h AEL) the expansion of interstitial length is constant throughout the arbor (Figure 2C). Interestingly, this growth pattern of major dendrites was not altered in the *Tbcc* mutant. Altogether, this propose that the distal region of the arbor exhibit more expansion and active growth at early time points, and limitation of tubulin assembly dominantly affects the growth and placement of terminal dendrites.

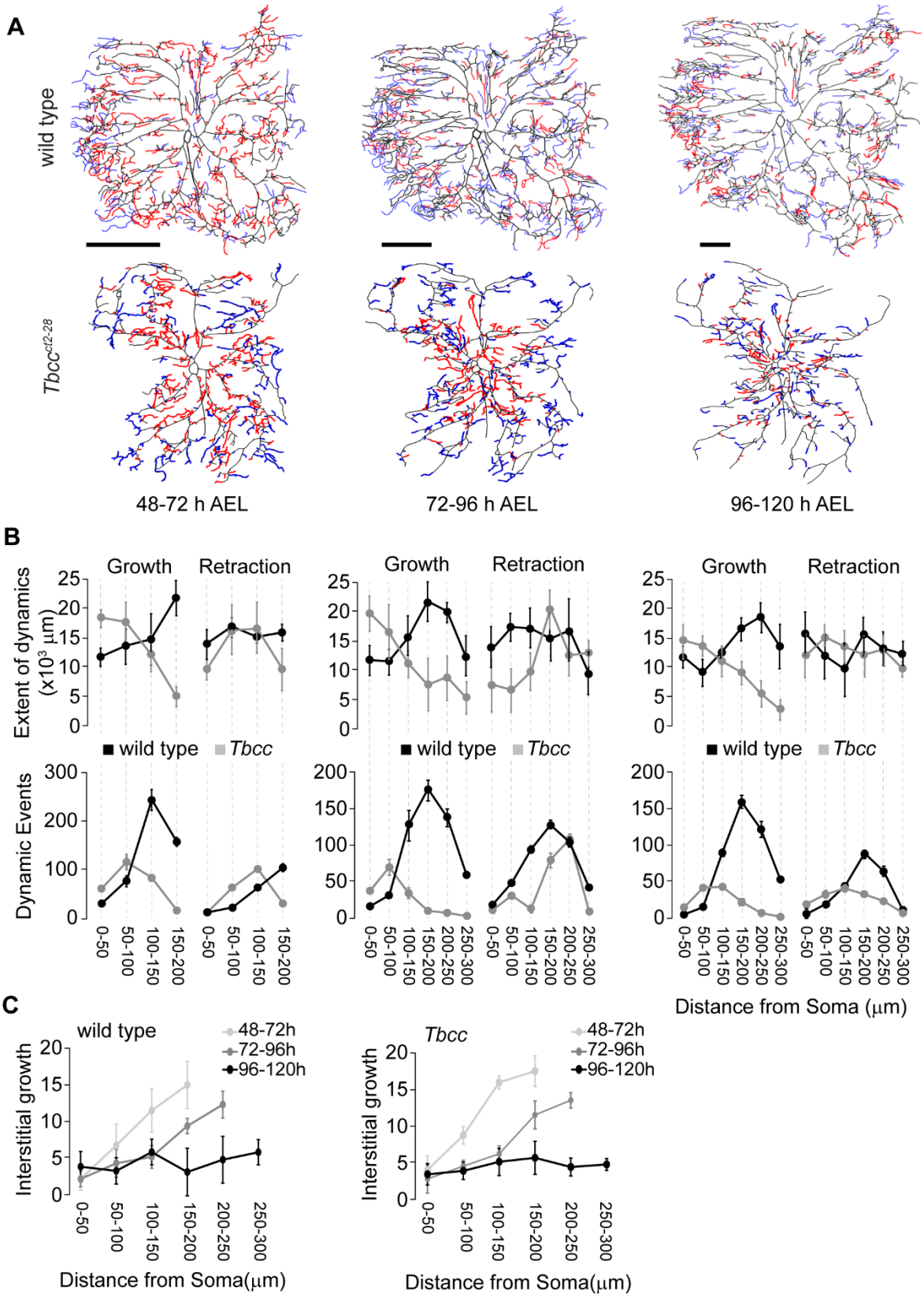
A
wild type
Tbcc^ct2-28
48-72 h AEL
72-96 h AEL
96-120 h AEL
B
Growth
Retraction
Extent of dynamics (x10^3 µm)
wild type
Tbcc
Dynamic Events
0-50
50-100
100-150
150-200
200-250
250-300
Distance from Soma (µm)
C
wild type
Tbcc
48-72h
72-96h
96-120h
Interstitial growth
Distance from Soma(µm)

Figure 2. Profile of growth and retraction in developing neurons. Montage was created with camera lucida tracings of an identical MARCM clone of c4da neuron images at 48h, 72h, 96h, and 120h AEL, overlapped with each former time point. Terminal branches were marked red for the portion that grew and blue for retracted (A). Branch length of each category as growth and retraction was measured in 50μm increment bins according to the distance from the soma, and plotted as extent of dynamics, or the number of events (B). Interstitial length difference of the major branch was measured and plotted with the same distance bins in WT and *Tbcc*. Scale bars: 50μm, error bars stand for standard deviation, n=6 for each time points and genotype.

We decided to directly measure the tubulin dynamics by Fluorescence Recovery After Photobleaching (FRAP) of EGFP tagged alpha-Tubulin. Because the growth profile was different in major dendrites and terminal dendrites by developmental course, we measured the % of recovery in each type of dendrites, grouped 50μm bins from the soma (Figure 3A), at early and late phase of development. In the case of major dendrites, at the early phase of development (48h AEL) there was a bias as the measuring point locating more distal: there was an increased percentage of fluorescence recovery in respect of the control experiment with soluble GFP (Figure 3B). Interestingly, this pattern was correlative with the regional bias of active growing (Figure 2), suggesting the growth of dendrite is resulting from the higher dynamics of tubulin. In contrast, as the development progresses to 120 AEL, this bias is no longer observed, as the tubulin recovery is uniformed when normalized to the soluble GFP. The prominent decrease of soluble GFP is presumably reflecting the difference of free diffusion rate of the molecules, given the diameter of the dendrites decrease by distance. On the other hand, terminal dendrites at 48h AEL shown a slight decrease as the region shift distally (Figure 3C), however at 120h AEL the

pattern is reversed as the tubulin recovery increase in the more distal regions (Figure 3D). This is the first deliberate measurement of tubulin dynamics in a living dendrite, with resolution of different dendritic regions, which is the distance from soma and hierarchy of dendrite branches, and also of the developmental course.

As it was revealed that there are indeed different dynamics of tubulin in different regions of the dendrite, we further investigated whether a specific region of the dendrite contributes more on tubulin supply in a longer time scale using photoconvertible alpha tubulin. EosFP emits strong green fluorescence (516 nm) that changes to red (581 nm) upon UV irradiation at 405 nm because of a photo-induced modification involving a break in the peptide backbone next to the chromophore (Wiedenmann et al., 2004). We expressed an N-terminus tagged tdEosFP alpha tubulin in the C4da neurons and photoconverted different regions of the main dendrite. Due to low quantum yield and poor persistency, we were not able to photoconvert and track movement in the terminal dendrites, but only in the main dendrites: specifically in interstitial regions (Figure 3E) or the branchpoints (Figure 3G), at 48h AEL or 120h AEL. We first imaged the entire dendrite arbor with 488nm emission, then photoconverted 8μm ROIs with 405nm UV laser, then recovered the larva into an individual cell with food, then re-imaged the same larval segment after 4 hours with both 488nm and 533nm. Movement of tubulin was measured as the line distance of converted magenta signal that traveled further than the initial ROI boundary. As a control, soluble EosFP was used to evaluate the simple diffusion in different regions of the dendrite. In the interstitial zone, at early development, there was more travel of the tubulin as the distance from soma increases (Figure 3F), which is again reflecting the active growth on that region, whereas at late developmental stage this bias in travel distance does not show anymore. In contrast, from the branchpoints of the dendrite, there was no significant

difference of movement by the distance from soma at the early stage of development, but at 120h AEL there was a dramatic increase of travel distance that peaks at 201~300 μm from the soma (Figure 3H). In every measurement point there was no significant difference within the travel distance of soluble Eos control. This non-uniformed tendency implies that the travel distance measurement does reflect the tubulin supply transition within dendrite regions, and the dominant site shift from interstitial region to branchpoints, notably towards the distal region of branchpoints. Taken the observation from FRAP and photoconversion of tubulin experiments together, we could conclude that within a dendrite there are compartmentalized zones of tubulin supply/assembly activity and the major site of this activity shifts from the distal interstitial regions to the distal branchpoints as development progress and the dendrite maintains its shape.

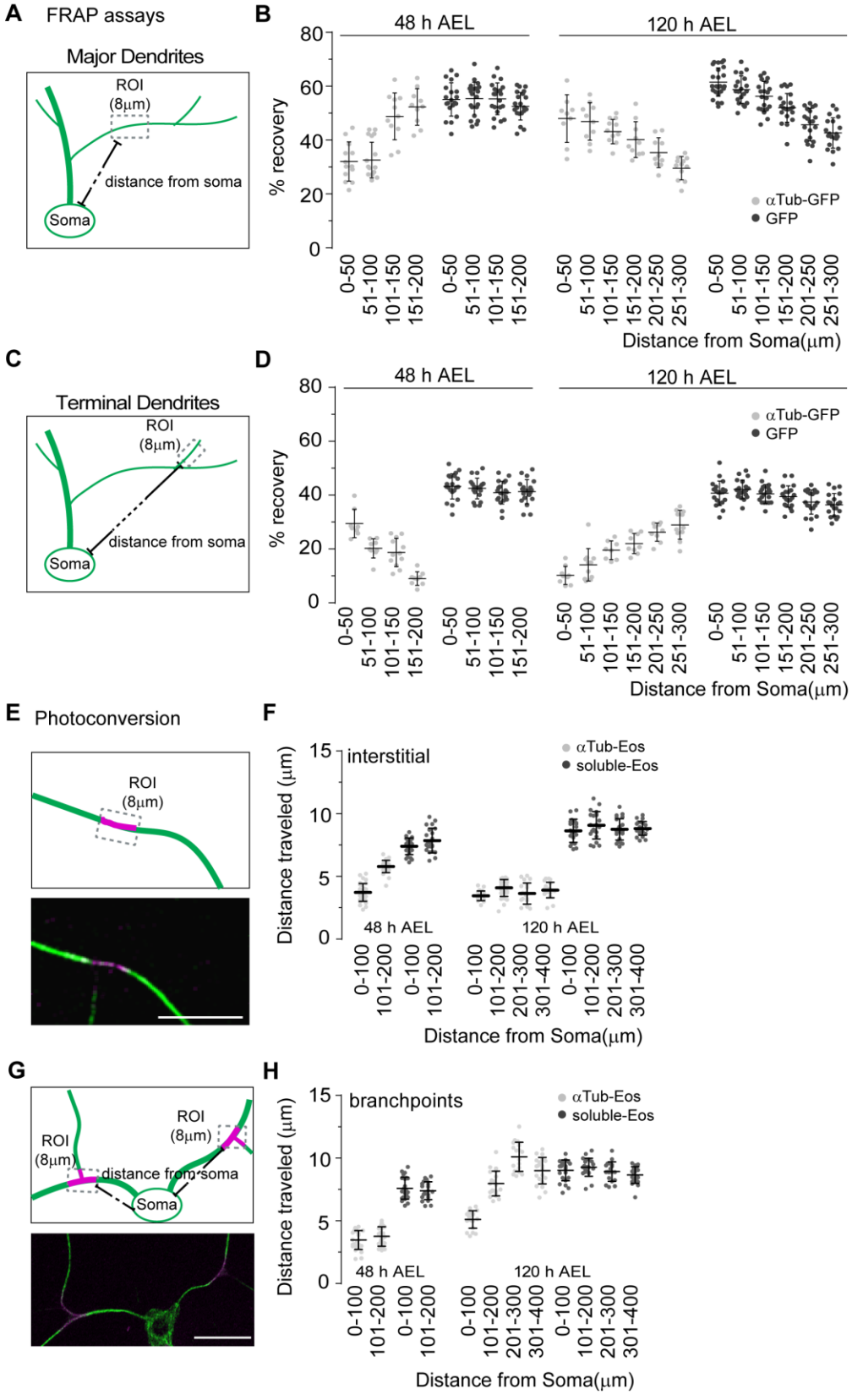
A
FRAP assays
Major Dendrites
ROI
(8μm)
distance from soma
Soma
B
48 h AEL
120 h AEL
% recovery
αTub-GFP
GFP
0-50
51-100
101-150
151-200
201-250
251-300
Distance from Soma(μm)
C
Terminal Dendrites
ROI
(8μm)
distance from soma
Soma
D
48 h AEL
120 h AEL
% recovery
αTub-GFP
GFP
Distance from Soma(μm)
E
Photoconversion
ROI
(8μm)
F
interstitial
αTub-Eos
soluble-Eos
Distance traveled (μm)
48 h AEL
120 h AEL
0-100
101-200
201-300
301-400
Distance from Soma(μm)
G
ROI
(8μm)
ROI
(8μm)
distance from soma
Soma
H
branchpoints
αTub-Eos
soluble-Eos
Distance traveled (μm)
48 h AEL
120 h AEL
Distance from Soma(μm)

Figure 3. Measuring tubulin dynamics and determining the major site of tubulin supply. (A-B) Percent of recovery was measured as the mobile fraction FRAP of αTubulin-GFP and soluble GFP within each 50μm increment bins according to the distance from the soma at 48h and 120h AEL, in major dendrites (A) and terminal dendrites (C). 8μm was selected for Region of interest (ROI) and for each measurement the power of UV laser was controlled so it bleached approximately 40% of the initial brightness. (B, D) Scatter plot showing % of recovery. (E-H) 8μm of either interstitial region (F) or branchpoints (H) were selected as ROI and photoconverted with 405nm UV laser, then imaged after 4 hours and the distance that traveled from its initial position was measured. Error bars indicate standard deviation (n>16 for αTubulin-GFP and n>20 for soluble GFP; n>25 for αTubulin-Eos and n>20 for soluble Eos).

Golgi outpost (GOP) have been known to localize selectively to dendritic branchpoints to confer arborization as a part of a satellite secretory pathway containing endoplasmic reticulum and GOP; the number and location of these organelles locally influences dendrite growth and dynamics (Aridor et al., 2004) (Ye et al., 2007). Since we discovered that the dendritic branchpoints are the major region that contribute to tubulin supply at later stage of development, we decided to investigate if the local GOP positioning is altered in *Tbcc* mutants. We co-expressed GFP tagged Grasp65 to label trans-Golgi with membrane targeted RFP in C4da neurons, and observed the number of distinct GFP puncta and measured the distance from soma of each puncta (Figure 4A-B). Initially at 48h AEL, GOP is not present in the dendrites. At 72h AEL and 96h AEL, the distribution of GOP is indistinguishable between wild type and $Tbcc^{ct228}$. However, at 120h AEL, the number of GOP in $Tbcc^{ct228}$ is greatly reduced, and the distribution is accumulated towards the soma.

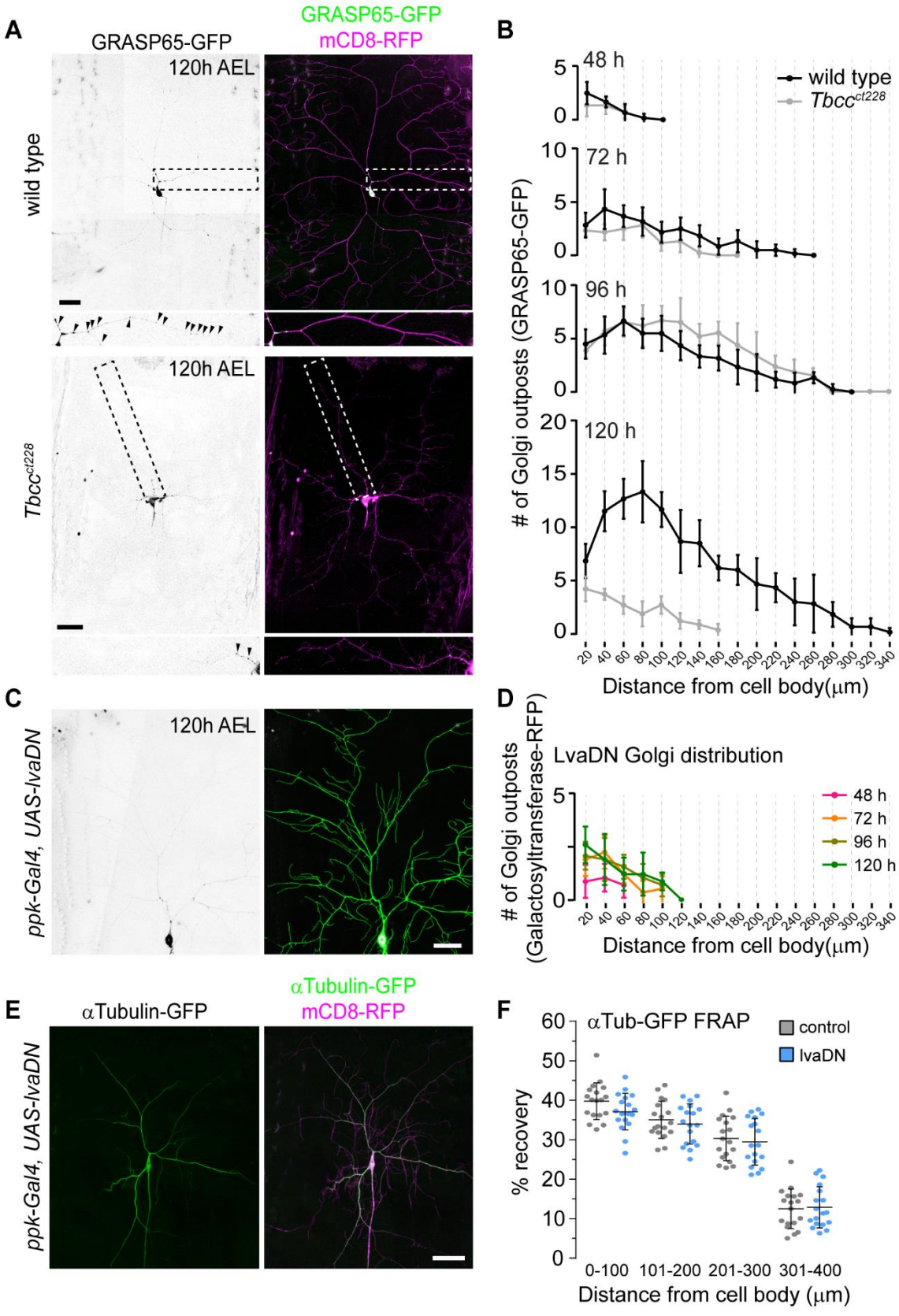
A
GRASP65-GFP
GRASP65-GFP
mCD8-RFP
120h AEL
wild type
120h AEL
Tbcc^ct228
B
48 h
72 h
96 h
120 h
wild type
Tbcc^ct228
# of Golgi outposts (GRASP65-GFP)
Distance from cell body(μm)
C
120h AEL
ppk-Gal4, UAS-IvaDN
D
LvaDN Golgi distribution
48 h
72 h
96 h
120 h
# of Golgi outposts (Galactosyltransferase-RFP)
Distance from cell body(μm)
E
αTubulin-GFP
αTubulin-GFP
mCD8-RFP
ppk-Gal4, UAS-IvaDN
F
αTub-GFP FRAP
control
IvaDN
% recovery
0-100
101-200
201-300
301-400
Distance from cell body (μm)

Figure 4. Distribution of Golgi outpost is misplaced and accumulated towards the soma. (A-B) Membrane of c4da MARCM clone was labeled with mCD8-RFP and distribution of Golgi was monitored by Grasp65-GFP in wild type and *Tbcc*$^{ct2\text{-}28}$. Distribution of GFP puncta was measured with sholl analysis (B). Dominant negative form of Lavalamp (Lva) was expressed with *ppk* driver with membrane GFP to label the morphology of the dendrite (C), and the distribution of Golgi was measured with sholl analysis (D). FRAP of αTubulin-GFP within each 100μm increment bins according to the distance from the soma at 120h AEL, with or without LavDN expression (E-F). Error bars indicate standard deviation (n=6 for Golgi distribution, n=16 for each FRAP experiments).

The distribution shift of GOP, interestingly, is observed approximately 24h later than the phenotype of *Tbcc*^{ct228} manifest, which suggests that the GOP may not be the major contribution to the phenotype, for at least the early phenotypic effects. To check if this effect was simply derived from GOP mislocation, we restricted the transportation of GOP by expressing dominant negative form of Lavalamp (LvaDN) (Papoulas, Hays, & Sisson, 2005)in C4da neurons. First, we confirmed that LvaDN effectively works, and retention of GOP was confirmed at all stages of larval development (Figure 4C-D). Next, we measured the tubulin dynamics using the same FRAP method as Figure 2, to check if the retrieval of GOP influence the dynamics of tubulin in the dendrites. Recovery rate was assessed in 100μm bins of distance from soma, at 120h AEL. Despite the expression of LvaDN had never allowed GOP localization in the dendrites, the tubulin dynamics were comparable with wild type. This indicates that GOP is not the essential factor for establishing tubulin dynamics in the dendrite, and suggests a distinct mechanism to regulate tubulin dynamics in different regions of dendrite in different developmental timing.

Tubulin specific chaperones function together as a tubulin assembly machinery, coupling the α- and β-tubulin subunits into a tightly associated heterodimer (Tian & Cowan, 2013). TBCC, which functions in final assembly of the two subunits and also in discharging the native α/β heterodimer, was one of the genes that was identified from our phenotypic screen with two separate alleles. As the other mutants that had the similar dendritic shift phenotype turned out to have shared cellular function in tubulin assembly, we hypothesized the regulation of tubulin assembly might be the factor that was critical for dendritic tubulin dynamics' change that is associates with growth. $Tbcc^{ct2\text{-}28}$ was identified to have a single nucleotide mutation that caused 26Tyr to become early stop codon, and $Tbcc^{gubana}$ was mapped to have two missense mutation in the Spectrin-like domain and in the region following immediately after the domain. Since there were more available genetic tools we decided to focus on the $Tbcc^{ct2\text{-}28}$ mutant. Both alleles of *Tbcc* had the dendrite shift phenotype to the comparable degree (Figure 5A-B), and the phenotype was fully rescued to the wild type level when mutant clones were re-supplied with UAS-TBCC-GFP (Figure 5C). Overexpression of TBCC-GFP in c4da neurons with *ppk* driver did not show any noticeable effects (Figure 5D), in dendrite distribution, total dendrite length, and the number of terminal dendrites (Figure 5F-G). We initially intended to observe the tubulin dynamics in the *Tbcc* mutant, however we confirmed that the tubulin structure was disintegrated from even 48h AEL (Figure5 H-I). So we decided to investigate the role of TBCC protein in terminal dendrite growth.

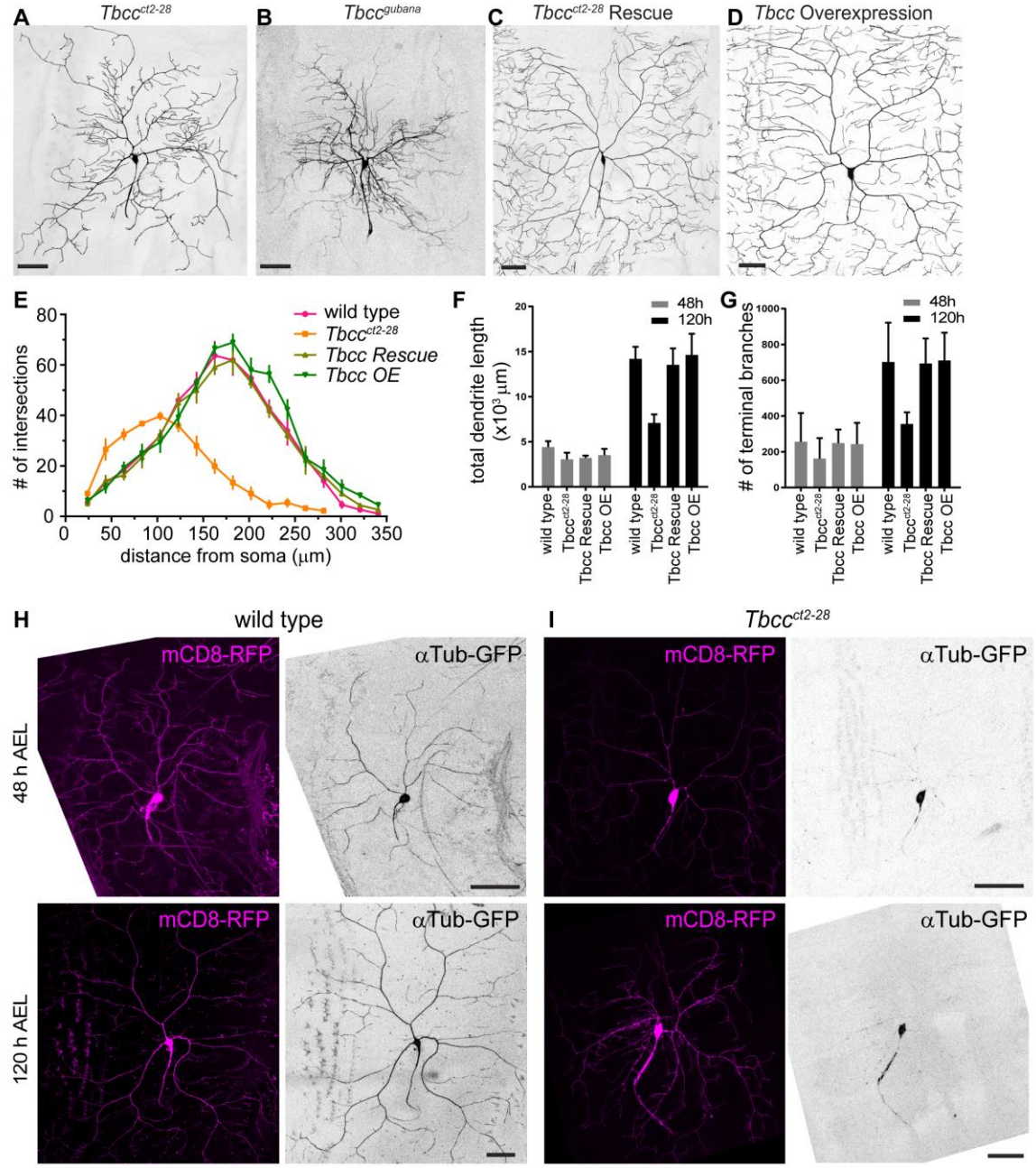

Figure 5. Phenotype of *Tbcc* mutants (A-B) are fully restored by UAS-TBCC-GFP expressed with 109(2)80-gal4 driver in MARCM clones (C), and the overexpression of UAS-TBCC-GFP with *ppk* driver did not show a significant morphological change (D). Sholl analysis depicting the distribution intersections at 120 AEL (E) (n=6). Average terminal dendrite length (F) and average number of terminal branches (G) for 48h AEL and 120h AEL; error bars indicate standard deviation. Tubulin integration is severely disrupted in *Tbcc*$^{2-28}$ from the early stage of development (H-I).

Distribution of TBCC-GFP was uniformly distributed over the arbor even from 48h AEL (Figure 6A), and the number of the TBCC-GFP puncta is maintained over the course of development (Figure 6B). Approximately 60% of the branchpoints contain TBCC-GFP, whereas 5% and 12% contains Golgi outpost at 48h AEL and 96h AEL, respectively. Majority of the branchpoints that contain Golgi outposts also had TBCC-GFP puncta, and more than half of the branchpoints contains solely TBCC-GFP (Figure 6C).

To understand the active role of TBCC associated to terminal branch dynamics, we monitored the behavior of terminal branch categorized as grow, retract, and stable (Figure 6D) after 4 hours of development, in the branchpoints that contain or not contain TBCC-GFP puncta. Terminal dendrites that contain TBCC puncta were likely to either grow or retract (33.05%, 12.66%, respectively), and the branchpoints absent with TBCC were more shifted to retract (4.50% to 26.66%) (Figure 6E). As to further confirm TBCC is positively regulating terminal branch growth, we blindly applied UV laser to the branchpoints, and monitored the dynamics after laser treatment. The profile of dynamics that had contained TBCC-GFP puncta shifted from growth and stable to increased retraction, whereas the profile of that not contained TBCC-GFP puncta was grossly unchanged (Figure 6F). We next monitored the direct evidence of microtubule growth with monitoring end binding protein EB1. Interestingly, TBCC-GFP and EB1-RFP majorly overlapped with each other (Figure 6G). Number of EB1-RFP puncta per terminal branch was similar whether or not containing TBCC-GFP. Among those EB1, there were about 2-fold increase of the mobile fraction in the branches that contained TBCC-GFP, indicating the presence of TBCC located at branchpoints can promote growth of microtubule in terminal dendrites (Figure 6H).

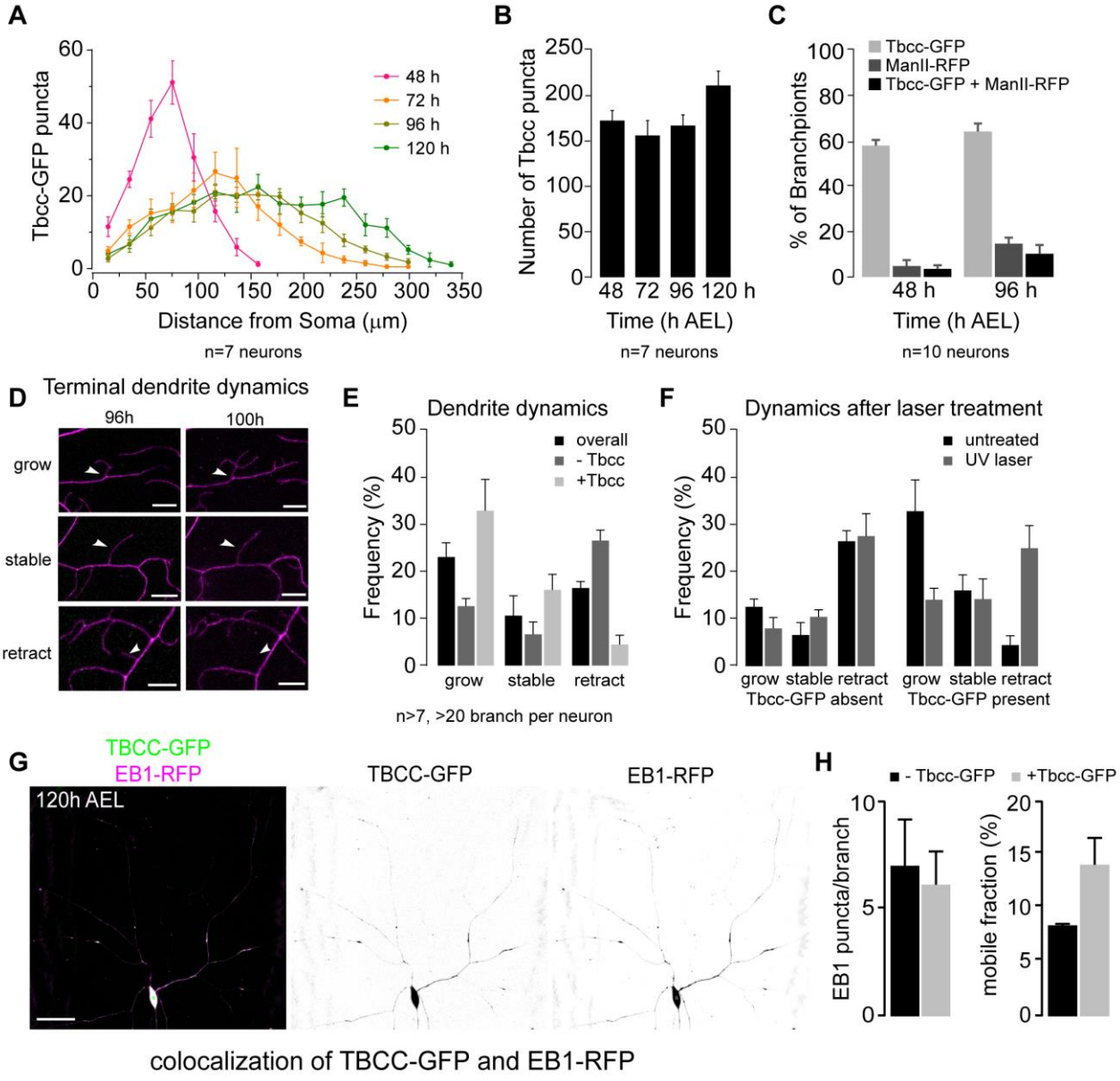

colocalization of TBCC-GFP and EB1-RFP

Figure 6. Presence of TBCC at branchpoints correlated with growth dynamics of the terminal branches. Sholl analysis depicting the distribution of TBCC-GFP at 48h, 72h, 96h, and 120 AEL (A) (n=6). Total number of TBCC-GFP is maintained globally throughout development (B). TBCC and GOP overlap increases by time, but the majority of TBCC are still not co-localized (n=20) (C). Presence of TBCC on the base of terminal branches (D) correlated with dynamic growth (n=28 branches) (E). Treatment of UV laser promotes retraction selectively on terminal branches that contain TBCC puncta. (n=13) Majority of EB1-RFP and TBCC-GFP co-express with *ppk*-driver overlap on the arbor of the dendrite (G). Number of EB1 puncta per terminal branch and the mobile fraction of those EB1 puncta (n=13) (H). Error bars indicate standard deviation.

CHAPTER 2.

Coordinate control of terminal dendrite patterning and dynamics by the novel membrane protein Raw

Identification of mutations that affect dendrite compartmentalization

To identify the developmental bases for compartment-specific patterning in dendrites, we used mosaic analysis with a repressible cell marker (MARCM) to screen for mutations that differentially affected different regions of C4da dendrite arbors (Lee and Luo, 1999). From this screen, we identified two phenotypic groups that define different levels of organization of dendrite arbors. First, we identified a group of mutant alleles that differentially affected terminal dendrite growth/placement along a proximal-distal axis relative to the cell body (Fig. S1). In wild type C4da neurons, terminal dendrites are concentrated at the distal (relative to the soma) region of the arbor, whereas mutants of this group affected distribution of terminal dendrites along the proximal-distal axis. Most commonly, as seen in *jj565* mutant neurons, mutants in this group caused exuberant terminal dendrite branching in proximity to the soma and a drastic reduction in terminal dendrites in the distal regions of the dendrite arbor (Fig. S1). Notably, this phenotype is similar to dendrite phenotypes caused by mutations in *dlic* (Satoh et al., 2008; Zheng et al., 2008), thus we hypothesize that organization along the proximal-distal axis involves microtubule-based transport. Consistent with this hypothesis, *jj565* is an allele of *dynactin p65*. Second, we identified a large group of mutants that preferentially affect patterning of terminal dendrites without affecting growth or patterning of major dendrites. Within this group we identified mutants that affected the number, length, and/or orientation of terminal dendrites. For example, *jj491* caused a simplification of terminal arbors; *jj835* mutants were completely devoid

of terminal dendrite arbors; and *jj599* mutants affected the placement of terminal dendrites, with terminal dendrites frequently crossing over one another, but not the average length of terminal dendrites (Fig. S1). The identification of mutants that are required for formation of terminal dendrite arbors (*jj835*) and distinct aspects of terminal patterning (length, *jj491*; placement, *jj599*) suggest that multiple pathways function at different levels of control to pattern terminal dendrites. At the outset of our screen, we anticipated that we should be able to identify mutations that selectively affect primary dendrite growth, however we have not identified any such mutations, possibly indicating that primary dendrite growth is a prerequisite for terminal dendrite branching (Parrish et al., 2006). Nevertheless, results from our screen suggest that dendrite arbor development in C4da neurons is compartmentalized in at least two different ways: growth of terminal dendrites along a proximal-distal axis emanating from the cell body, and in patterning of main and terminal dendrites.

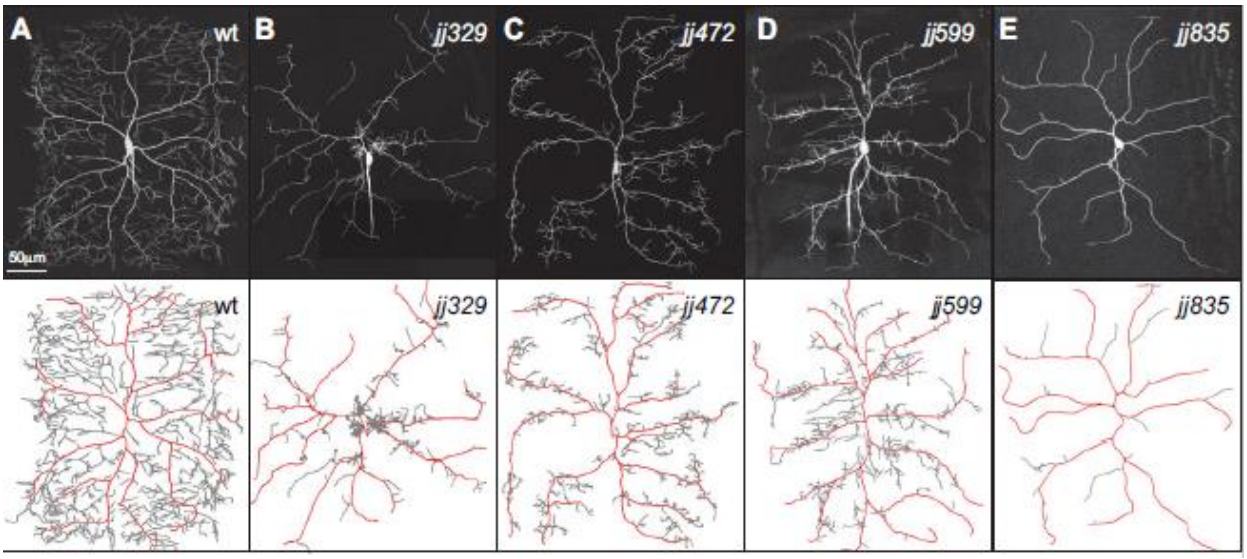

Figure S1. Genetic screen for mutants that define different modes of dendrite compartmentalization. Representative C4da MARCM clones are shown for the following: (A) wild type (wt) control, (B) *jj329*, which affects proximal-distal positioning of dendrite branches, (C) *jj472*, which affects elongation of terminal dendrites but not major dendrites, (D) *jj599*, which affects terminal dendrite placement and elongation but not major dendrite patterning, and (E) *jj835*, which is required for growth of terminal dendrites but not major dendrites. Traces below clones depict major dendrites in red and higher order dendrites in gray.

Table S1. Genetic Screen for compartmentalization in dendrites

	Chromosome 2L, Frt 40A	**Chromosome 2R, Frt 42D**
Overview		
Lines screened	1800	1055
Lethal mutations screened (empirically determined)	2880	1580
Lines with dendrite phenotypes	60	31
Phenotypic breakdown		
Growth/stability of entire arbor	24	10
Proximal/distal branch placement	9	3
Terminal dendrite elongation	28	16
Terminal Dendrite number	30	17
Terminal dendrite crossing	7	3

Numbers reflect the number of alleles in each class, according to the (qualitative) isolation phenotype. Note that many alleles score positive for more than one defect; that is, in some lines, multiple phenotypes co-occur (as in *raw* mutants).

***raw* regulates multiple aspects of terminal dendrite patterning**

Among the group of mutants that preferentially affected terminal dendrites, *jj102* was of particular interest because it affected multiple aspects of terminal dendrite patterning, including terminal dendrite branching, length, and orientation, suggesting that it may define a point of convergence for multiple signaling pathways that influence terminal dendrites (Fig. 1). Since *jj102* appeared to define a control point for terminal dendrite patterning, we chose to characterize it in detail. Compared to wild type C4da neurons, *jj102* mutant C4da neurons exhibited four characteristic terminal dendrite defects. First, terminal dendrites branched directly off of major dendrites in *raw* mutants, whereas branches emanating from major dendrites in control neurons branched extensively. Thus, although the total branch number and distribution of branch points along major dendrites were similar in *raw* mutants and wild type controls, *raw* mutants neurons exhibited reduced complexity in distal regions of the arbor, which normally contain highly branched dendrites (Fig. 1E). Additionally, the path length from the soma to terminal dendrite tip was, on average, significantly shorter in *raw* mutants (Fig. 1F). Second, the average length of terminal dendrites was significantly reduced in *raw* mutants (Fig. 1G). As a result, the total dendrite length was reduced in *raw* mutant neurons as well. Third, the placement of terminal dendrites was altered: both the branch angle and 3D placement of terminal dendrites were defective in *jj102* mutants. In wild type neurons, branch angles of terminal dendrites approached 90°, but terminal dendrites of *raw* mutants branched at acute angles (Fig. 1H). As a result, terminal dendrites often grew in close proximity to primary dendrites, rather than growing away from them. In addition, dendrite-dendrite crossing events were rampant in *jj102* mutant neurons, with terminal dendrites crossing over one another significantly more frequently than in controls (Fig 1B', I). Thus, *raw* defines a point of convergence for developmental control of multiple aspects of terminal dendritogenesis.

To characterize the molecular basis for these defects we set out to identify the gene affected by *jj102*. Homozygous *jj102* mutants arrest as embryos with dorsal closure defects, and using meiotic mapping we localized *jj102* to a small interval on chromosome 2 that contained one gene with a known

function in dorsal closure, *raw* (Nusslein-Volhard, C. et al., 1984). Consistent with *jj102* affecting *raw* function, chromosome deficiencies that uncover *raw* and reduction-of-function alleles in *raw* (*raw*^{1}, *raw*^{lex1}, *raw*^{k01021}) failed to complement the lethal phenotype of *jj102*, and a lethal P-element insertion in the *raw* locus previously implicated in patterning of the peripheral nervous system phenocopied the dendrite defects of *jj102* (Fig. 1C, 1F-I) (Kania et al., 1995; Prokopenko et al., 2000). Finally, we found that *jj102* carried a nonsense mutation in the *raw* coding sequence (CAA->TAA, Q777Stop in Raw short; see below), which should lead to a premature stop prior to a predicted trans-membrane domain (Fig. 1J) (Jones et al., 1994).

To establish that the *jj102* dendrite defects were caused by loss of *raw* function, we used MARCM to resupply functional *raw* to *jj102* mutant neuron clones. To this end, we generated a transgene encoding a GFP-Raw fusion protein (*UAS-GFP-raw*, Fig. 1J) using the short isoform of *raw*, which has been implicated in PNS development (Prokopenko et al., 2000). *UAS-GFP-raw* fully rescued the terminal dendrite patterning defects of *jj102* mutant C4da neurons, including the simplification of terminal arbors, reduction in mean terminal branch length, and the increase in terminal dendrite crossing (Fig. 1D, 1F-I). By contrast, overexpressing UAS-GFP-raw in wild type C4da neurons had no effect on terminal branch patterning (data not shown), thus raw is necessary for terminal dendrite patterning but not sufficient to promote exuberant growth. Altogether, these results demonstrate that raw functions cell-autonomously to regulate terminal dendrite orientation and elongation, and that Raw-short can support dendrite development; we have not investigated the function of other isoforms in the PNS.

Figure 1. *raw* is required for terminal dendrite patterning

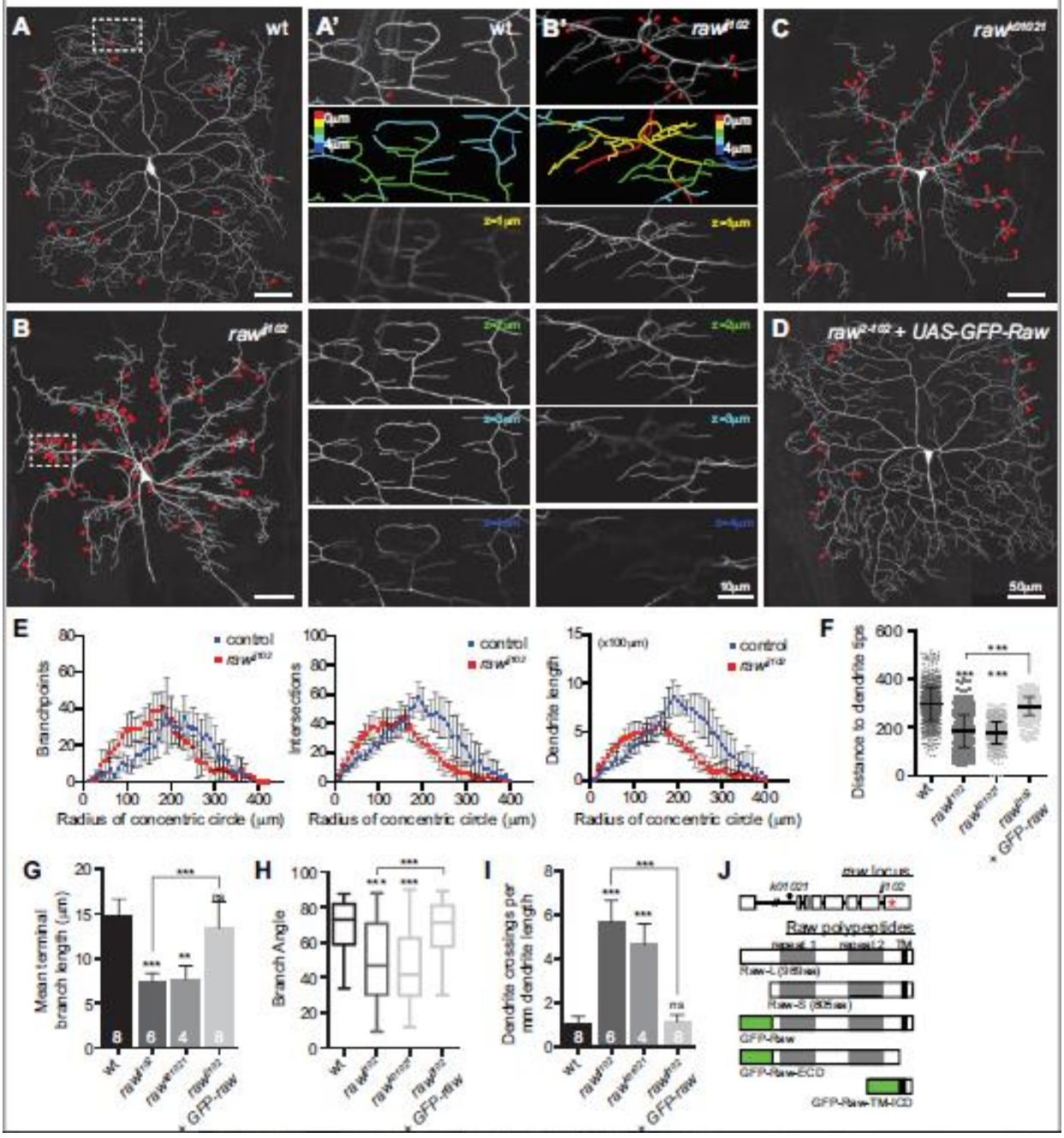

Figure 1. Raw affects terminal dendrite patterning.

Representative MARCM clones for wild type (wt) control (A), *raw*^{jj102} (B), *raw*^{k01021}, (C) and *raw*^{jj102} + *UAS-GFP-Raw* (D). Arrowheads mark dendrite-dendrite crossings. Axial position of terminal dendrites in control (A') or *raw*^{jj102} mutant neurons are shown for regions marked by hatched boxes. (E-I) Morphometric analysis of dendrites from C4da MARCM clones of the indicated genotypes. (E) Sholl analysis depicting distribution of branch-points, intersections, and dendrite length. (F) Scatter plot showing path lengths from the cell body to branch endings. Data points, measurements from a representative neuron; error bars, aggregate mean and 95% confidence interval. (G) Average terminal branch length; error bars, standard deviation. (H) Terminal branch angles; box plots depict mean values and 1st/3rd quartile, whiskers mark minimum/maximum values. (I) Dendrite-dendrite crossing, normalized to total dendrite length. Error bars, standard deviation. ns, not significant, *p<0.05, ***p<0.001 relative to control; one way ANOVA with post-hoc Dunnett's test. Scale bars: 10 μm for (B'), 50 μm for other panels. The number of neurons analyzed for each genotype is indicated in (I). (J) Schematic of the *raw* locus, predicted polypeptides, and *GFP-Raw* constructs. *k01021* carries a *P{lacW}*insertion, and *jj102* carries a missense mutation in the last coding exon. Raw has two ~100 amino acid repeats of unknown function and a putative C-terminal transmembrane domain.

Raw promotes terminal dendrite stabilization

Homozygous *raw* mutant embryos arrest before dendrite outgrowth begins in the PNS and *raw* influences development of a variety of embryonic tissues (Byars, Bates, & Letsou, 1999; Jack & Myette, 1997; Jemc, Milutinovich, Weyers, Takeda, & Van Doren, 2012) (Kania et al., 1995), therefore to ascertain the developmental origin of the raw mutant dendrite defects, we monitored dendrite phenotypes of raw mutant MARCM clones during early larval development. At each stage we observed, (clones become visible in late 1st instar larvae), raw mutant neurons exhibited characteristic terminal branching defects while major dendrites grew comparable to controls, thus raw is required for dendrite development from early stages of larval development and appears to act primarily on terminal dendrites.

The *raw* mutant terminal dendrite branching defects could reflect a failure in terminal branch elongation, increased rates of terminal branch retraction, or some combination of both. To determine the cellular basis for the terminal dendrite defects of *raw* mutant neurons, we monitored terminal dendrite dynamics in wild type or *raw* mutant C4da neuron single cell MARCM clones using time-lapse microscopy. Initially, we chose a 4-hour window of development after larval growth is nearly complete and C4da dendrite arbors are no longer expanding. During this 4-hour time lapse, beginning at 96 hours after egg laying (AEL), the majority of terminal dendrites of C4da neurons exhibit dynamics, but the extent and frequency of branch extension and retraction are nearly equivalent (Fig. 2A, 2C-E). By contrast, a significantly larger proportion of terminals exhibited dynamics in *raw* mutant neurons, with the dynamic branches retracting more frequently than they grew, unlike wild type controls (Fig. 2B, 2C-E). Additionally, the extent of dynamics was significantly different in *raw* mutants than wild type controls (1.8 μm for control neurons, 3.8 μm for *raw* mutant neurons, 96-100 hours AEL) (Fig. 2H). Thus, *raw* appears to regulate terminal dendrite stability.

Our developmental analysis of raw mutant neurons suggested that raw is required for stabilization of terminal branches throughout development. We therefore monitored dendrite dynamics over an earlier time-lapse when arbors are growing rapidly and adding new terminal dendrites. Between 72-76hr AEL, control neurons exhibited an increased frequency of dynamics and a different distribution of dynamics: terminal growth occurred almost twice as frequently as retraction during the early interval whereas growth and retraction occurred at equivalent rates during the late interval (Fig. 2C, D). As in the late time-lapse, raw mutants exhibited significantly more dynamic behavior than wild type controls between 72-76hr AEL (Fig. 2C). Notably, whereas dynamic behavior of control neurons changed over development, the rate of dynamics and the frequency of growth/retraction in raw mutant clones was similar over both time-lapses, suggesting that terminal dendrite growth is constantly offset by retraction in raw mutants (Fig. 2D). Thus, raw affects terminal branch stability; at each time-point examined, terminal dendrites of

raw mutants were more dynamic than controls, with growth matched by retraction. Hence, terminal dendrites of raw mutants rarely branch or elongate, preventing elaboration of terminal arbors.

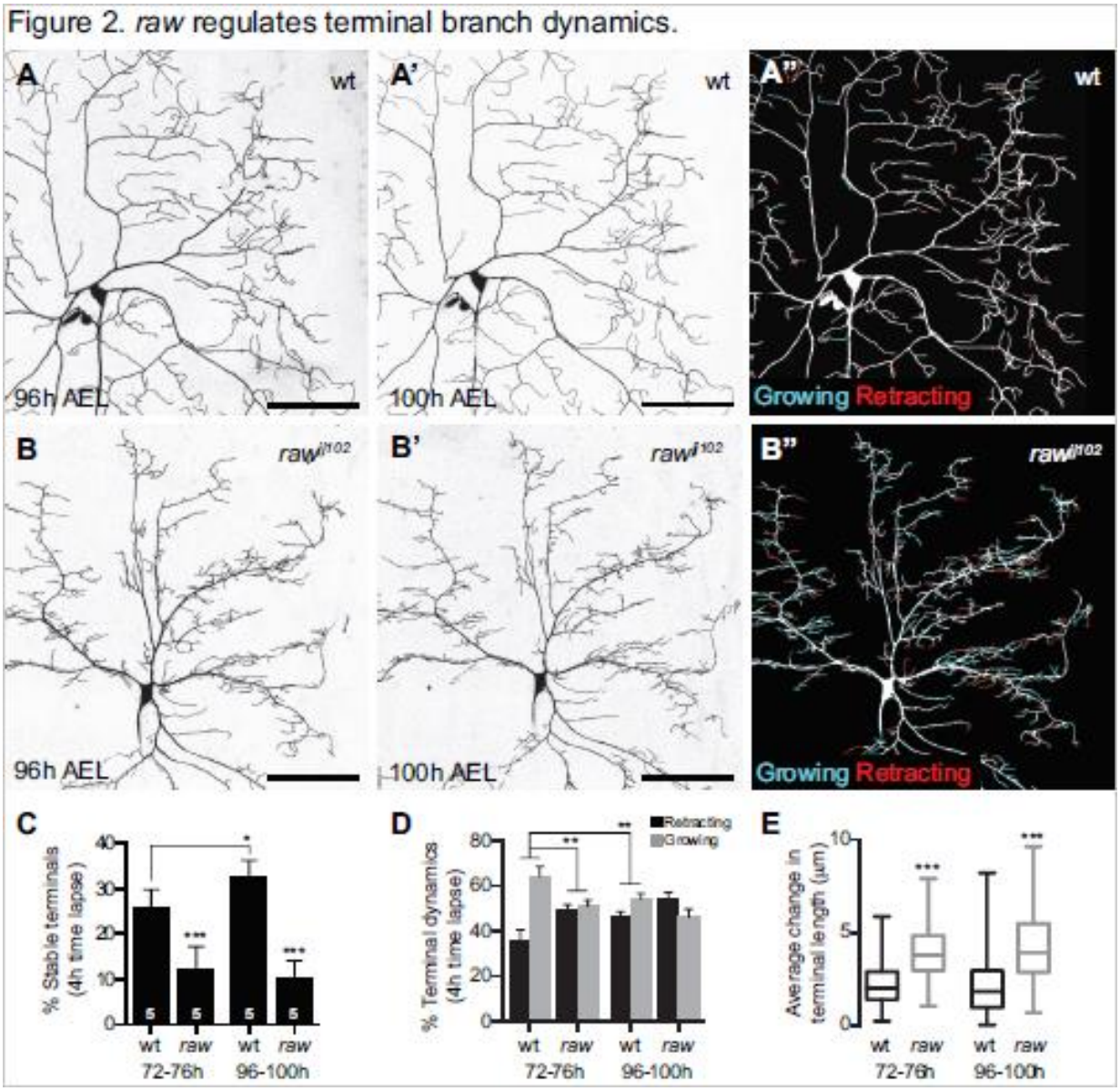

Figure 2. Raw regulates terminal branch dynamics.

Time-lapse analysis of terminal dendrite dynamics. Control ddaC MARCM clone imaged at 96hr (A) and 100hr AEL (A') to monitor terminal dendrite dynamics. (A") Growth (cyan) and retraction (red) are pseudocolored in a composite of the two time-points. (B) Time-lapse images of a raw^{jj102} ddaC MARCM clone. (C-E) Quantification of terminal dendrite dynamics (72-76hr or 96-100hr AEL) in wt and raw^{jj102} MARCM clones. *n=5* neurons, each genotype. The proportion of (D) stable and (E) dynamic (retracting, black; growing, gray) terminals is shown. Error bars, standard deviation. (E) Change in terminal dendrite length for dynamic terminals. Box plots depict mean values and 1st/3rd quartile, whiskers mark minimum/maximum values. **p<0.01, ***p<0.001; ns, not significant; one way ANOVA with post-hoc Dunnett's test in (C) and (E), binomial test in (D).

Raw may function locally in dendrites to regulate terminal dendrite patterning

To gain insight into the mechanism by which Raw regulates terminal dendrite dynamics, we monitored the intracellular distribution of Raw by expressing GFP-Raw in *raw* mutant C4da neuron clones. In these clones, GFP-Raw is the only functional Raw protein, thus we reasoned that GFP-Raw localization would likely reflect Raw's site of action. As described above, GFP-Raw rescues the terminal dendrite patterning defects of raw^{jj102} or raw^{k10104} mutant C4da MARCM clones. In dendrites, GFP-Raw is concentrated in puncta, most of which localize to branch-points along major dendrites (Fig. 3A, green arrowheads), consistent with Raw locally regulating terminal dendrite patterning. However, GFP-Raw signal was rarely detectible in distal dendrites or at dendrite tips, suggesting that Raw may function at branch-points to stabilize nascent dendrites or to recruit other factors that function in dendrite terminals, for example factors that promote microtubule invasion. Terminal dendrites are rapidly turned over in *raw* mutants, therefore we monitored whether GFP-Raw localization correlated with terminal branch stabilization. Using time-lapse microscopy, we monitored dendrite dynamics during an 18-hour interval in *GFP-Raw* expressing raw^{jj102} mutant C4da MARCM clones and examined whether presence of GFP-Raw

puncta at branch-points was associated with branch stabilization (Fig. 3B). We sampled more than 500 dynamic terminal dendrites from 6 different neurons and found that growth behavior of terminal dendrites originating in branch-points containing GFP-Raw ($\chi^2 = 23.80$, df = 2, $p < 0.01$) or lacking GFP-Raw ($\chi^2 = 14.90$, df = 2, $p < 0.01$) was significantly different from the population of terminal dendrites as a whole. Specifically, branches associated with GFP-Raw puncta were significantly more likely to grow or remain the same length and less likely to retract, whereas branches originating in branch points lacking GFP-Raw were more likely to retract, consistent with Raw promoting terminal dendrite stabilization/elongation (Fig. 3C).

Alternative splicing of *raw* gives rise to multiple isoforms with different N-terminal exons and a common C-terminus that contains a putative transmembrane domain (Byars et al., 1999; Daines et al., 2011) (Graveley et al., 2011) (Jones et al., 1994). Thus, we reasoned that *raw* may encode a membrane protein that coordinately regulates multiple aspects of terminal dendrite development in response to extracellular cues. To test this possibility, we first investigated whether Raw is membrane-associated. To this end, we fractionated S2 cells transfected with *UAS-GFP-Raw* and probed the cellular fractions with antibodies to GFP, alpha-tubulin (cytoplasmic marker) and Robo (membrane marker). Indeed, we found that GFP-Raw was present in the cytoplasmic and membrane fractions, demonstrating that some of the GFP-Raw was membrane-associated (Fig. 4A). Similarly, the *C. elegans* Raw ortholog (Olrn-1) is membrane-associated, but Olrn-1 has multiple putative transmembrane domains not present in Raw (Bauer Huang et al., 2007). Our membrane topology prediction suggested that the N-terminal ~700 amino acids of Raw comprised an extracellular domain, whereas the short C-teminus was located intracellularly (Jones et al., 1994). We therefore examined the distribution and topology of Raw using surface staining of "rescued" *raw* mutant MARCM clones expressing GFP-Raw, reasoning that GFP should be exposed on the cell surface if Raw is targeted to the plasma membrane. As a negative control, we first assayed for surface exposure of GFP in MARCM clones expressing EB1-GFP, a microtubule-associated protein that should not be surface-exposed. Although EB1-GFP was dispersed throughout the dendrite arbor, no

surface staining of GFP was evident, demonstrating that the plasma membrane of C4da neurons was not permeabilized in our staining protocol (Fig. 4B). By contrast, C4da neurons expressing GFP-Raw exhibited punctate GFP surface staining (Fig. 4C), and these puncta frequently occurred at dendrite branch-points. Similarly, we observed GFP surface staining in S2 cells expressing GFP-Raw (data not shown). We conclude that Raw can associate with membranes and that the N-terminal domain can be exposed to the extracellular environment at branch-points where Raw may locally influence terminal dendrite development.

Figure 3. Raw accumulates at branchpoints of persistent dendrites

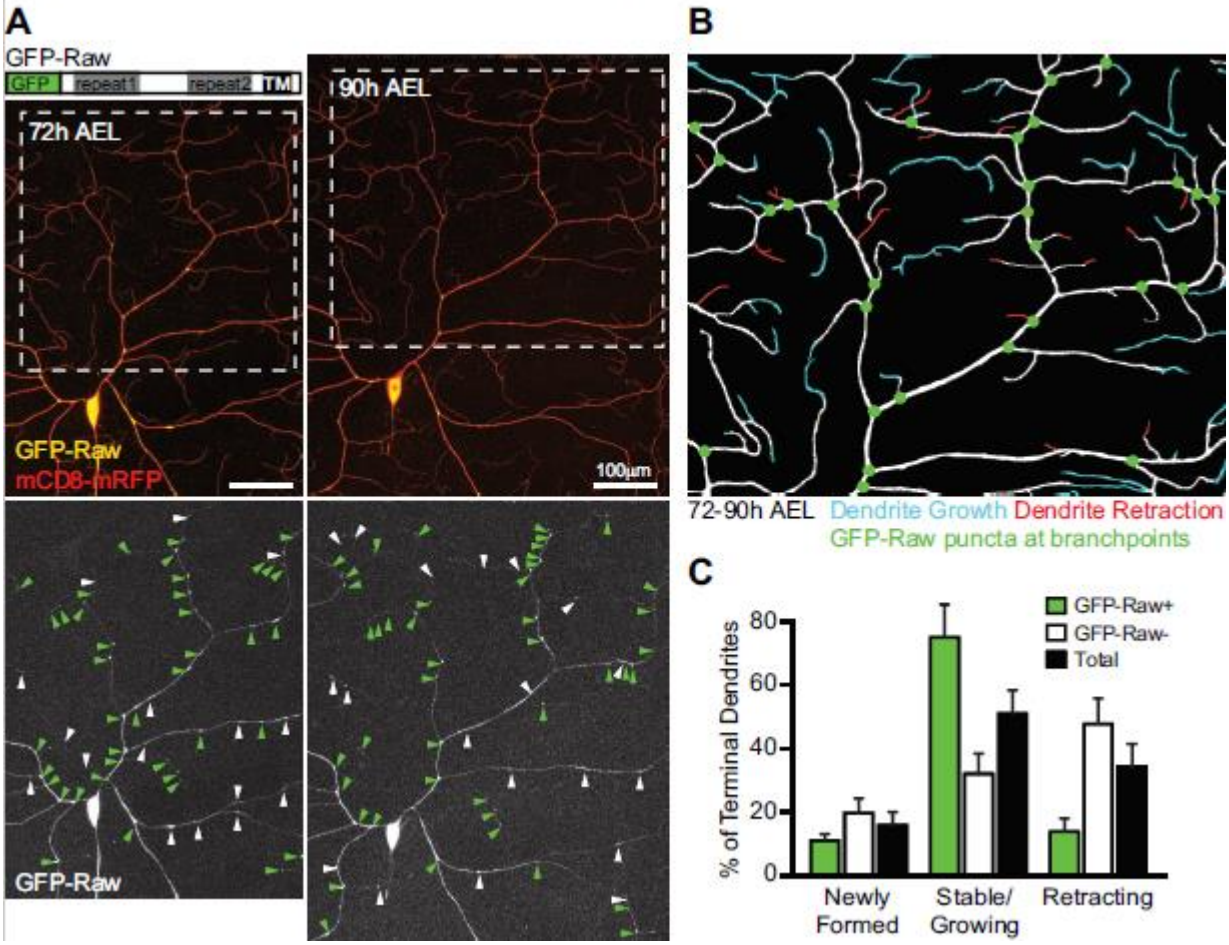

Figure 3. Raw accumulates at branch-points of persistent dendrites.

(A) Time-lapse imaging of *raw*^{j102} C4da neuron MARCM clone expressing *UAS-GFP-Raw*, which rescues *raw*^{j102} dendrite defects. The same neuron is imaged at 72hr and 90hr AEL. *Top*, merge of GFP-Raw (yellow) and mCD8-mRFP (red) signals. *Bottom*, GFP-Raw distribution. Arrowheads mark GFP-Raw puncta; green, branch-point localized puncta; white, puncta in interstitial regions. (B) Trace of region of interest (box in A) depicting dynamic terminal dendrites (red, retracting; cyan, growing) and GFP-Raw puncta localized at branch-points (green). 3/18 retracting terminals emanate from GFP-Raw containing branch-points. (C) Quantification of dynamics for terminal dendrites emanating from branch-points containing GFP-Raw puncta (green), branch-points lacking GFP-Raw puncta (white), or all branch-points (black). *n*=6 clones; ~100 terminals were scored in each clone.

Figure 4. Raw is a cell surface protein

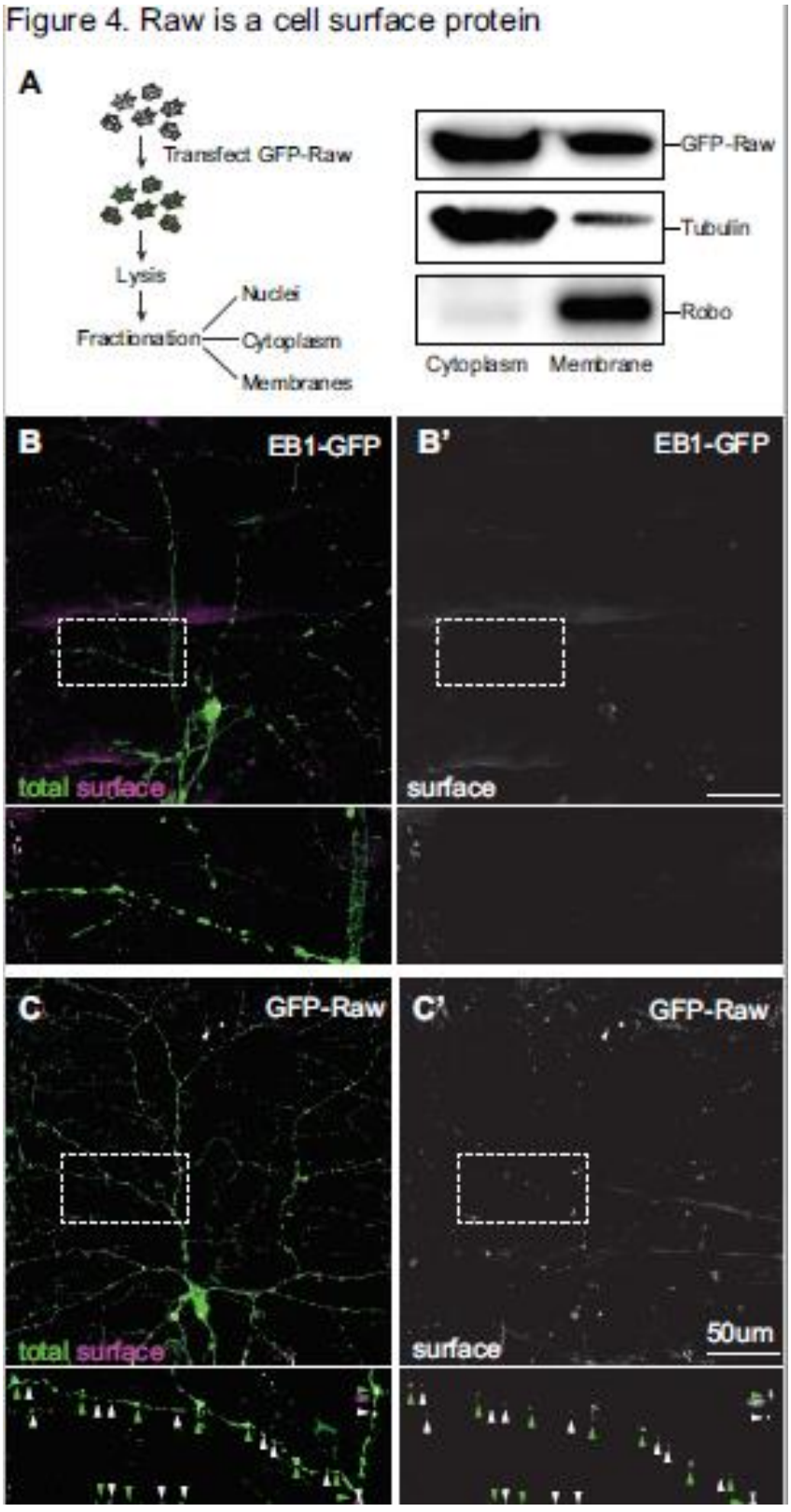

Figure 4. Raw localizes to the plasma membrane. (A) Raw associates with membranes in S2 cells. Left, Cell fractionation workflow. Right, Western blot of Cytoplasm and Membrane fractions probed with GFP (GFP-Raw), Tubulin (Cytoplasm) and Robo (Membrane) antibodies. (B-C) GFP-Raw localizes to the dendritic plasma membrane. Total GFP fluorescence after fixation (B) and surfaceexposed GFP revealed by immunostaining under non-permeabilizing conditions (B') for a wild type C4da MARCM clone expressing UAS-EB1-GFP. Total GFP fluorescence after fixation (C) and surface exposed GFP-Raw (C') for a raw^{j102} C4da neuron MARCM clone expressing UAS-GFP-Raw. Zoomed images, region of interest boxed in images above. Arrowheads, GFP-Raw puncta; green arrowheads, puncta at branch-points. Additional puncta likely localize to branch-points, but we cannot unambiguously identify all branch-points with this fixation protocol. Scale bars, 50 μm.

raw interacts with the trc pathway to regulate terminal dendrite adhesion

We next set out to characterize downstream pathways by which Raw regulates terminal dendrite patterning. In dorsal closure and gonadal ensheathment, raw negatively regulates Jnk signaling to modulate cell-cell interactions (Byars et al., 1999) (Jemc et al., 2012). We hypothesized that raw similarly regulates Jnk signaling in C4da neurons to pattern terminal dendrites. We therefore monitored effects of raw on phospho-Jnk accumulation, on expression of the JNK pathway target puckered, and on AP-1 reporter expression in C4da neurons (Chatterjee & Bohmann, 2012), and in each case we observed no effect. Likewise, modulating JNK activity had no obvious effect on C4da dendrite patterning. We therefore conclude that raw likely signals through distinct pathways in the epidermis and C4da neurons, with raw function in dendrite patterning being largely independent of Jnk signaling.

To identify genes that function with raw to regulate terminal dendrite patterning, we assayed for genetic interactions between raw and known regulators of terminal dendrite development, including genes in the Trc signaling pathway, which regulate dendrite-dendrite repulsion and terminal dendrite adhesion; turtle (tutl), which regulates dendrite-dendrite repulsion; Dscam, which regulates dendrite self-avoidance; and myespheroid (mys), which is required for dendrite-ECM interactions (Emoto et al., 2004) (Han et al., 2012) (Kim, Jan, & Jan, 2012) (Koike-Kumagai, Yasunaga, Morikawa, Kanamori, & Emoto, 2009) (Long, Ou, Rao, & van Meyel, 2009). On its own, heterozygosity for mutation in raw or any of the other genes had no significant effect on the number of terminal dendrite crossing events, but larvae doubly heterozygous for mutations in raw and Trc signaling pathway genes exhibited significant increases in dendrite-dendrite crossing (Fig. 5), suggesting that Raw functions together with the Trc pathway to regulate terminal dendrite patterning. Similar to raw, trc regulates multiple aspects of terminal dendrite patterning, namely terminal dendrite number and adhesion, and these activities are genetically separable (Emoto et al., 2004). However, we observed significant changes in dendrite crossing but not dendrite number in raw/trc double heterozygotes, suggesting that the different functions of raw in terminal branching are likewise genetically separable, with terminal dendrite adhesion involving trc.

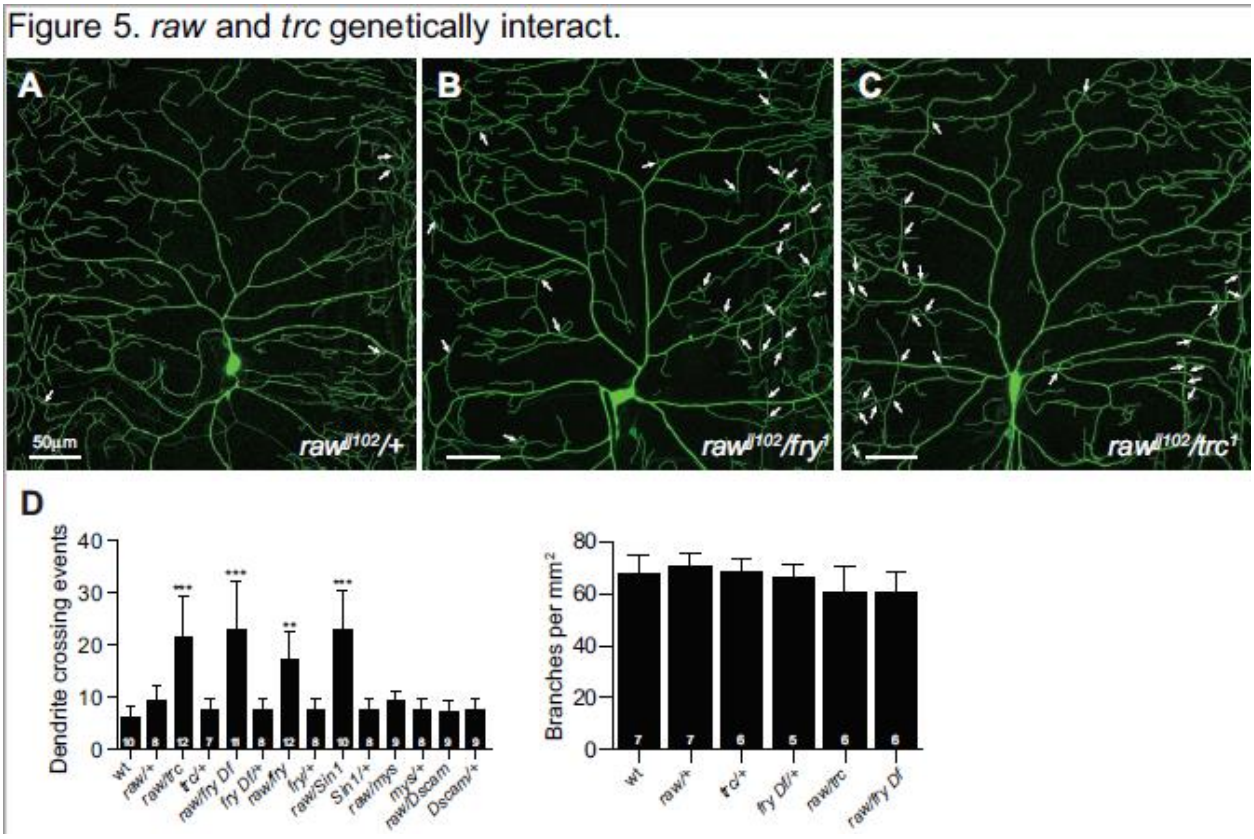

Figure 5. Raw and Trc genetically interact.

(A-C) C4da dendrites visualized using *pickpocket::mCD8-GFP* in *raw*^{ji102}/+ heterozygous (A) *raw*^{ji102}/*fry*^{1} double heterozygous (B) and *raw*^{ji102}/*trc*^{1} double heterozygous (C) larvae. (D) Quantification of dendrite crossing phenotypes and dendrite branch number. Error bars, standard deviation; *p<0.05, **p<0.01, **p<0.001; one way ANOVA with post-hoc Dunnett's test.

Next, we assayed for physical association between Raw and Trc. To this end, we co-expressed GFP-Raw and Trc-mCherry-HA in S2 cells and examined whether the epitope tagged proteins co-immunoprecipitated. Indeed, Raw co-immunoprecipitated with Trc and vice-versa (Fig. 6A), and a truncated Raw protein containing the transmembrane domain and intracellular domain (TM-ICD) interacted with Trc, whereas the Raw extracellular domain (ECD) did not (Fig. 6B). Trc activation is potentiated by membrane association (Hergovich, Bichsel, & Hemmings, 2005) (Koike-Kumagai et al., 2009), thus our findings that Raw is a membrane-associated protein, that Raw physically associates with Trc, and that the Raw TM-ICD mediates this interaction suggested that Raw might play some role in Trc phosphorylation/activation. To assess the functional relevance of the Raw-Trc interaction, we developed antibodies that allowed us to monitor Trc phosphorylation on threonine 449 (T449), the residue associated with maximal kinase activation (Fig. 6C) (Tamaskovic, Bichsel, Rogniaux, Stegert, & Hemmings, 2003). First, we examined the relationship between Raw and Trc activation in S2 cells. In control or GFP-Raw transfected S2 cells, Trc P-449 was present at low levels (Fig. 6D), suggesting that Raw is not sufficient to promote Trc phosphorylation. To examine whether Raw could facilitate Trc phosphorylation, we treated S2 cells with okadaic acid (OA) and monitored Raw's effect on Trc P-T449 accumulation. As expected, OA treatment induced Trc phosphorylation (Koike-Kumagai et al., 2009) (Millward, Hess, & Hemmings, 1999), and Raw overexpression led to a 62% increase in OA induced Trc phosphorylation (Fig. 6D). Thus, Raw can potentiate Trc activation in S2 cells. Further, Raw TM-ICD was sufficient to potentiate Trc phosphorylation whereas Raw ECD exhibited no activity in this assay (Fig. 6E), suggesting that Raw enhances Trc phosphorylation by promoting Trc membrane association/proximity.

To examine whether Raw influences Trc activity in vivo, we assayed effects of raw mutation on Trc phosphorylation in C4da neurons. In the larval PNS, Trc P-T449 immunoreactivity was present at high levels in C4da dendrites where it appeared to accumulate in puncta (Fig. 6F; rawjj102/+ heterozygote), consistent with prior reports that Trc is required for dendritic tiling in these neurons (Emoto et al., 2004). Trc P-T449 was also detectable in Class III da neurons, albeit at much lower levels, and trc is required for dendrite morphogenesis in these neurons as well (double arrowheads, Fig. 6F). Finally, Trc P-T449 was present at high levels in axons of da neurons (Fig. 6F, bracket). By contrast, in raw mutant C4da MARCM clones, Trc P-T449 levels were substantially reduced, to levels comparable to Trc P-T449 levels in Class III da neurons (Fig. 6G). Thus, raw appears to potentiate Trc phosphorylation in C4da neurons as well as S2 cells.

If raw functions through Trc to regulate dendrite-dendrite crossing, we reasoned, ectopic Trc activation in raw mutant neurons should mitigate the raw mutant dendrite crossing phenotype. This is what we found. Although overexpressing wild-type Trc in raw mutant neurons had a dominant-negative effect (Fig. 6H, J), overexpression of myristoylated Trc, which is membrane-targeted and hence constitutively active (Koike-Kumagai et al., 2009), significantly reduced dendrite-dendrite crossing in raw mutant neurons (Fig. 6I, J). Likewise, overexpression of a Trc phosphomimetic (UAS-Trc T449E) partially suppressed the raw mutant dendrite-dendrite crossing defect (Fig. 6J). Thus, the raw mutant dendrite-dendrite crossing defect is likely caused, in part, by deficits in Trc activation, which Raw may potentiate by promoting Trc membrane association.

Figure 6. Raw promotes Trc phosphorylation.

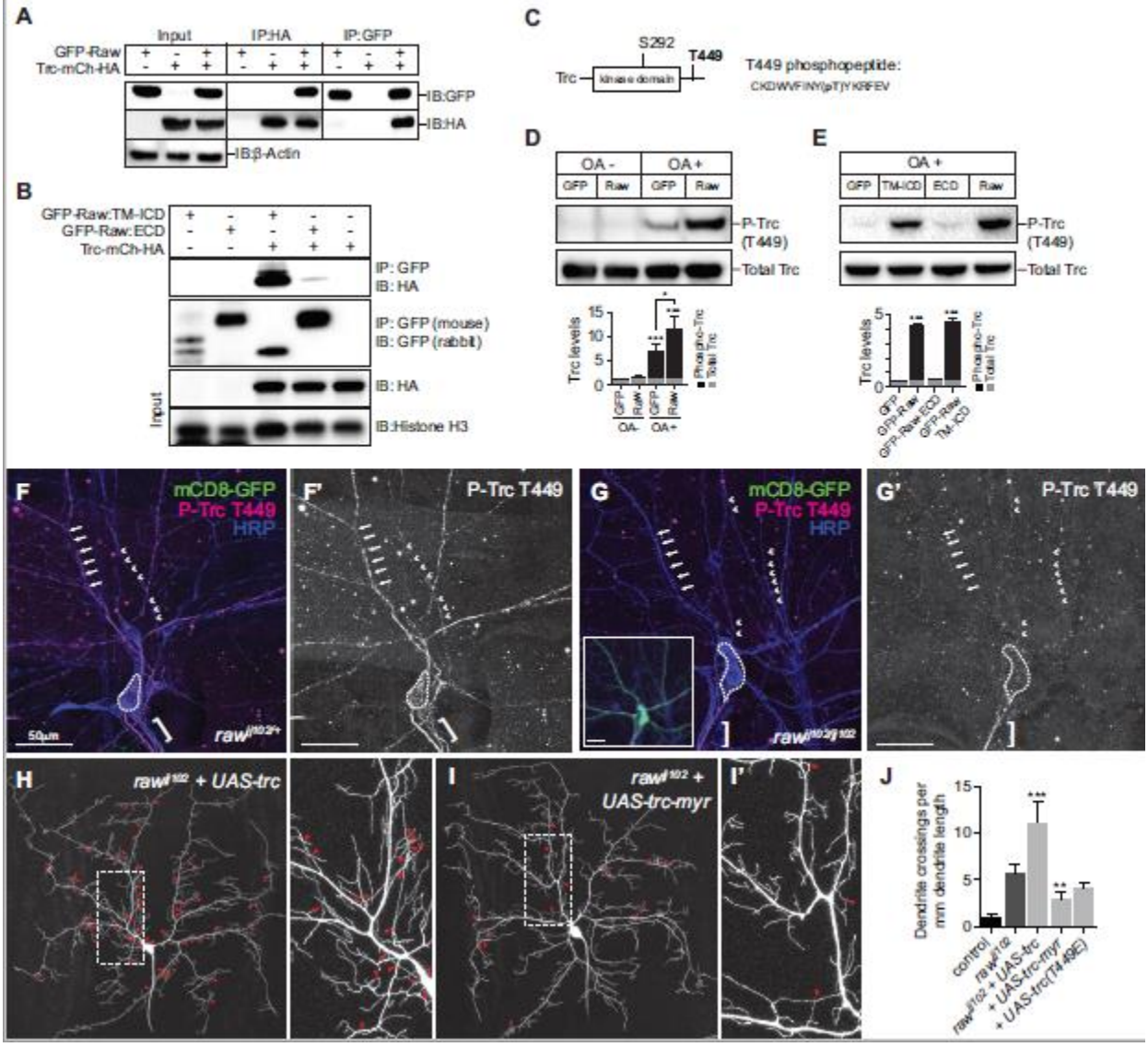

Fig. 6. Raw promotes Trc activation

(A-B) Raw-Trc association. Lysates of S2 cells transfected with *Trc-mCherry-HA* and/or (A) *GFP-raw* and (B) *GFP-Raw:TM-ICD* or *GFP-Raw:ECD* were immunoprecipitated (IP) and immunoblotted (IB) with the indicated antibodies. (C-E) Raw potentiates Trc phosphorylation. (C) *Left*, Trc schematic depicting phosphorylation sites; *right*, phoshphoepitope used to generate Trc P-T449 antibodies. (D) S2 cells were transfected with *GFP* or *GFP-raw* and Trc phosphorylation on T449 was assayed in the absence or presence of Okadaic Acid (OA) treatment using phospho-specific antibodies. Bar graph, mean levels (4 independent experiments) of total Trc (gray) and phospho-Trc (Black) in cell lysates. Error bars, standard deviation. (E) Raw TM-ICD fragment but not ECD fragment potentiates Trc phosphorylation. (F-G) Raw promotes Trc phosphorylation in C4da neurons. Immunostaining in raw^{jj102}/+ larvae carrying C4da $raw^{jj102/jj102}$ MARCM clones. Phospo-Trc (P-T449) immunoreactivity (magenta), anti-HRP to label sensory neurons (blue) and anti-GFP to label MARCM clones (inset, G) are shown. White hatched lines outline C4da cell bodies, brackets mark axons. (H-J) Raw promotes Trc activation to regulate dendrite-dendrite crossing. *UAS-trc* (H), *UAS-trc-myr* (I) or *UAS-trcT449E* (J) was expressed in raw^{jj102} C4da MARCM clones and effects on dendrite-dendrite crossing were analyzed (J). Arrowheads, dendrite-dendrite crossings. *p<0.05, **p<0.01, **p<0.001; one way ANOVA with post-hoc Dunnett's test.

Trc can modulate dendrite adhesion to the ECM (Han et al., 2012), therefore we investigated whether raw can likewise modulate adhesion. To this end, we compared adhesion of control or GFP-raw expressing S2 cells to different ECM components (Fig. 7A). GFP-raw expression significantly enhanced S2 cell adhesion to collagen and, to a lesser degree, fibronectin (Fig. 7B). Since Raw can modulate Trc activity, and one output of Trc is cell adhesion, we tested whether Raw promotes adhesion in a Trc-dependent manner. Indeed, a dominant negative version of Trc (Trc K112A) abrogated Raw's ability to enhance adhesion to collagen (Fig. 7C).

Since Raw promotes S2 cell adhesion to collagen with Trc and Trc promotes Integrin-based attachment of C4da dendrites to a collagen-rich ECM (Han et al., 2012), we examined whether defects in integrin-based adhesion contribute to the raw mutant dendrite phenotype. If raw modulates dendrite adhesion, we reasoned that increasing dendrite-ECM attachment should suppress the raw mutant dendrite-dendrite crossing defects, as integrin overexpression suppresses dendrite-dendrite crossing defects of Trc pathway mutants. To test this prediction, we assayed effects of neuronal overexpression of Integrins (UAS-mys + UAS-mew) on terminal dendrite patterning in raw mutant C4da MARCM clones. Integrin overexpression suppressed dendrite-dendrite crossings in raw mutant neurons (Fig. 7F), suggesting that dendrite-ECM attachment is compromised in raw mutants, and significantly increased terminal branch number (Fig. 7G), likely the result of stabilizing the exuberant, short-lived branches found in raw mutant C4da neurons. Indeed, Integrin overexpression altered raw mutant terminal dendrite dynamics, increasing the fraction of stable terminals (Fig. 7H).

However, Integrin overexpression did not rescue the raw mutant terminal dendrite elongation defect (Fig. 7I), suggesting that raw regulates branch stabilization and elongation via distinct mechanisms, with the former involving Trc.

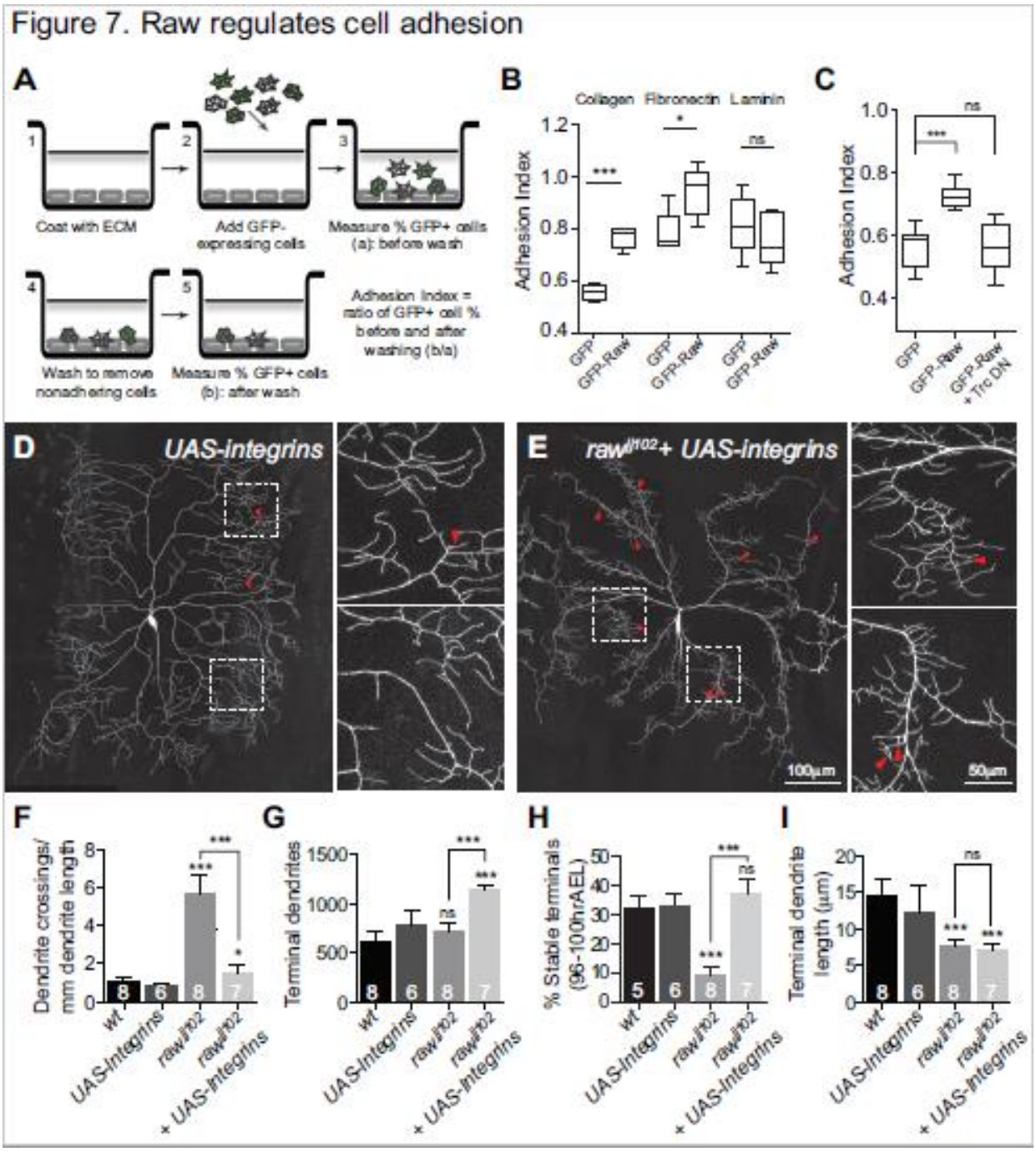

Figure 7. Raw modulates cell adhesion.

(A) S2 cell adhesion assay. (B) Cell adhesion to different substrates. S2 cells were transfected with *Actin-Gal-4* + *UAS-GFP* or *UAS-GFP-Raw*, and adhesion was assayed 2 days post-transfection. (C) Cell adhesion to Collagen was measured as in (B), but cells were additionally co-transfected with a dominant negative version of *Trc* (*Trc-DN; UAS-Trc K112A*). Box plots depict mean values and 1st/3rd quartile from 5 experiments (>100 cells scored for each experiment), whiskers denote maximum/minimum values. ns, not significant, *p<0.05, ***p<0.001 compared to *Actin-Gal-4* + *UAS-GFP* transfected S2 cells; student's t-test in (B), one way ANOVA with a post-hoc Dunnett's test in (C). (DG) Integrin-based adhesion promotes terminal dendrite stability. Overexpression of integrins (*UAS-mys* + *UAS-mew)* in a control (D) or raw^{ij102} C4da neuron (E). Arrowheads, dendrite-dendrite crossings. (F-I) Quantification of terminal dendrite crossings (F), number (G), dynamics (H) and length (I) in the indicated genotypes. The number of neurons analyzed for each genotype is indicated. ns, not significant, *p<0.05,***p<0.001 comared to *UAS-Integrins*; one way ANOVA with post-hoc Dunnett's test.

Coordinate regulation of terminal dendrite adhesion and elongation by *raw*

Raw modulates F-actin assembly in cuticular hairs (Blake, Myette, & Jack, 1999), and we noted that *raw* cell-autonomously regulated formation of actin-rich protrusions in oenocytes, suggesting that changes in actin assembly may contribute to the dendrite extension defects of *raw* mutants. To investigate this possibility, we monitored F-actin distribution using GMA-GFP in wild type and *raw* mutant C4da MARCM clones (Bloor & Kiehart, 2001). In wild type C4da dendrites, GMA-GFP was evenly distributed throughout the arbor with occasional concentrations at branch-points and in terminal dendrites. By contrast, terminal dendrites in *raw* mutant C4da neurons exhibited substantially higher levels of GMA-GFP than major dendrites. Thus, *raw*

mutant terminal dendrites appear to be enriched in F-actin, which likely contributes to the dynamic behavior of these terminals. We examined whether Raw physically interacts with Actin or Tubulin, but we were unable to detect either Actin or Tubulin in Raw immunoprecipitates (data not shown). We also found that *raw* had little effect on the dendritic microtubule cytoskeleton visualized with Tubulin-GFP. Thus, we conclude that Raw indirectly regulates cytoskeletal composition to influence terminal dendrite elongation. Consistent with Raw regulating branch elongation independent of the *trc/fry* pathway, we did not observe GMA-GFP accumulation in terminal dendrites of *fry* mutants. If indeed *raw* regulates terminal dendrite adhesion and elongation via distinct pathways, we reasoned that mutations in the signaling pathway(s) involved in branch elongation would selectively enhance the dendrite elongation phenotype of *raw* mutant neurons. To test this hypothesis, we screened our collection of terminal branching mutants for genetic interactions with *raw*. We identified one mutant (*jj472*) that genetically interacts with *raw* to affect terminal dendrite length and higher order branching without affecting the 3D orientation of terminal dendrites (Fig. 8A-C), further demonstrating that *raw* functions in terminal dendrite adhesion and elongation are genetically separable. Similar to *raw* mutant neurons *raw/ jj472* double heterozygotes had shorter terminal dendrites and less complex terminal arbors, thus the mean path length from the soma to branch endings was reduced in *raw/ jj472* double heterozygotes, as in *raw* mutant neurons (data not shown). On its own, homozygosity for *jj472* caused a significant decrease in terminal branch number and length, but only a modest increase in dendrite-dendrite crossing (Fig. 8D, E). *jj472* is loss-of-function allele of *AGO1*, which encodes an RNA-binding protein involved in miRNA-mediated translational repression (Forstemann, Horwich, Wee, Tomari, & Zamore, 2007), as *jj472* fails to complement $AGO1^{k00208}$ and $AGO1^{k08121}$, *jj472* carries a premature stop codon (Q319Stop) that

truncates AGO1before the catalytic domain (Hock & Meister, 2008), and *AGO1* RNAi and *AGO1*^{k08121} phenocopy the dendrite defects of *jj472* (Fig. 8F, G, data not shown).

Altogether, our results support model in which *raw* regulates terminal dendrite adhesion/stability and elongation by distinct pathways (Fig. 8J). Knockdown of one of these pathways causes terminal dendrite elongation defects (*AGO1-RNAi*, Fig. 8G) or dendrite-dendrite crossing defects (*trc-RNAi*, Fig. 8H), whereas knockdown of both pathways has an additive effect, resulting in dendrite defects similar to *raw* mutants (Fig. 8I). We have not yet characterized the *raw-AGO1* interaction in detail as *AGO1*overexpression causes severe patterning defects and occasional neuron death, and we have been unable to generate double mutant MARCM clones, so their respective functions in dendrite elongation remain to be determined. One possibility is that Raw interacts with AGO1 to influence local translation of key effectors of terminal dendrite growth as miRNAs regulate local translation in dendrites in some neurons (Vo, Cambronne, & Goodman, 2010), and several actors with roles in local translation affect terminal dendrite growth in C4da neurons (Olesnicky et al., 2014).

Figure 8. Coordinate control of dendrite adhesion and branch elongation by *raw*.

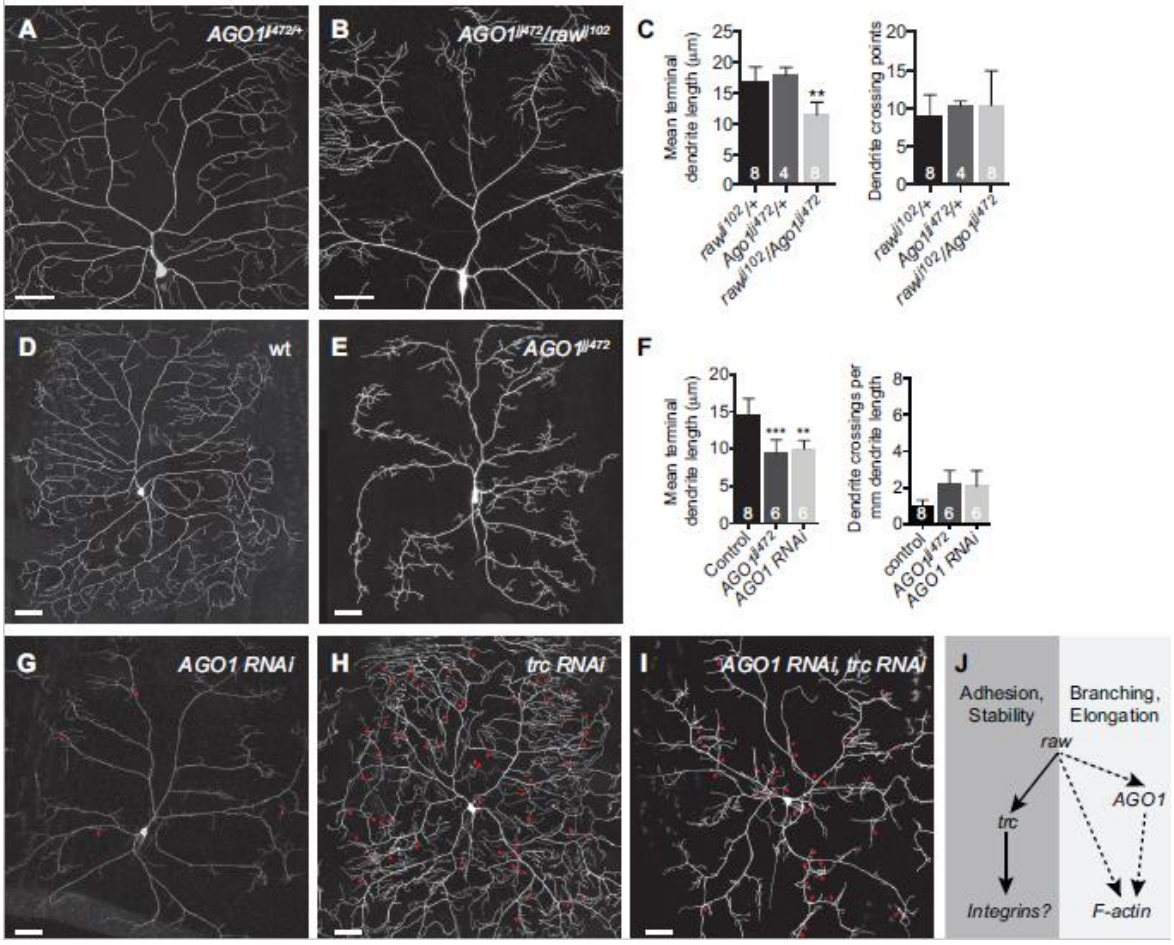

Figure 8. Coordinate control of terminal dendrite adhesion and elongation by *raw*.

(A-C) *AGO1* and *raw* genetically interact to regulate terminal dendrite length. Representative images of C4da neurons (*ppk-mCD8-GFP*) are shown for *AGO1^{ij472}*/+ (A) and *AGO1^{ij472}/raw^{ij102}* heterozygotes. (C) Mean terminal dendrite length and dendrite crossing points in larvae of the indicated genotypes. *Left*, Bar graph depicts mean of means; *Right*, bar graph depicts average number of dendrite-dendrite crossing points. The number of C4da neurons analyzed for each genotype is indicated. (D-F) *AGO1* regulates terminal dendrite growth. Representative C4da MARCM clones shown for wild type (wt) control (D) and *AGO1^{ij472}* (E). Scale bars, 50 µm. (F) Mean terminal dendrite length and crossing points for indicated genotypes. *p<0.05, ***p<0.001; one way ANOVA with post-hoc Dunnett's test. (G-I) Additive effects of *trc* and *AGO1* knockdown on dendrite patterning. (G) *UAS-AGO1-RNAi*, (H) *UAS-trc-RNAi*, or (I) *UAS-AGO1-RNAi + UAS-trc-RNAi*. (H) Genetic pathway for *raw* control of terminal dendrite patterning.

REFERENCES

Aridor, M., Guzik, A. K., Bielli, A., & Fish, K. N. (2004). Endoplasmic reticulum export site formation and function in dendrites. *J Neurosci, 24*(15), 3770-3776. doi:10.1523/JNEUROSCI.4775-03.2004

Baas, P. W., Deitch, J. S., Black, M. M., & Banker, G. A. (1988). Polarity orientation of microtubules in hippocampal neurons: uniformity in the axon and nonuniformity in the dendrite. *Proc Natl Acad Sci U S A, 85*(21), 8335-8339.

Bauer Huang, S. L., Saheki, Y., VanHoven, M. K., Torayama, I., Ishihara, T., Katsura, I., . . . Bargmann, C. I. (2007). Left-right olfactory asymmetry results from antagonistic functions of voltage-activated calcium channels and the Raw repeat protein OLRN-1 in C. elegans. *Neural Dev, 2*, 24. doi:10.1186/1749-8104-2-24

Blake, K. J., Myette, G., & Jack, J. (1999). ribbon, raw, and zipper have distinct functions in reshaping the Drosophila cytoskeleton. *Dev Genes Evol, 209*(9), 555-559.

Bloor, J. W., & Kiehart, D. P. (2001). zipper Nonmuscle myosin-II functions downstream of PS2 integrin in Drosophila myogenesis and is necessary for myofibril formation. *Dev Biol, 239*(2), 215-228. doi:10.1006/dbio.2001.0452

Byars, C. L., Bates, K. L., & Letsou, A. (1999). The dorsal-open group gene raw is required for restricted DJNK signaling during closure. *Development, 126*(21), 4913-4923.

Chatterjee, N., & Bohmann, D. (2012). A versatile PhiC31 based reporter system for measuring AP-1 and Nrf2 signaling in Drosophila and in tissue culture. *PLoS One, 7*(4), e34063. doi:10.1371/journal.pone.0034063

Chen, Y., & Sabatini, B. L. (2012). Signaling in dendritic spines and spine microdomains. *Curr Opin Neurobiol, 22*(3), 389-396. doi:10.1016/j.conb.2012.03.003

Daines, B., Wang, H., Wang, L., Li, Y., Han, Y., Emmert, D., . . . Chen, R. (2011). The Drosophila melanogaster transcriptome by paired-end RNA sequencing. *Genome Res, 21*(2), 315-324. doi:10.1101/gr.107854.110

Emoto, K., He, Y., Ye, B., Grueber, W. B., Adler, P. N., Jan, L. Y., & Jan, Y. N. (2004). Control of dendritic branching and tiling by the Tricornered-kinase/Furry signaling pathway in Drosophila sensory neurons. *Cell, 119*(2), 245-256. doi:10.1016/j.cell.2004.09.036

Forstemann, K., Horwich, M. D., Wee, L., Tomari, Y., & Zamore, P. D. (2007). Drosophila microRNAs are sorted into functionally distinct argonaute complexes after production by dicer-1. *Cell, 130*(2), 287-297. doi:10.1016/j.cell.2007.05.056

Fujishima, K., Horie, R., Mochizuki, A., & Kengaku, M. (2012). Principles of branch dynamics governing shape characteristics of cerebellar Purkinje cell dendrites. *Development, 139*(18), 3442-3455. doi:10.1242/dev.081315

Gardiol, A., Racca, C., & Triller, A. (1999). Dendritic and postsynaptic protein synthetic machinery. *J Neurosci, 19*(1), 168-179.

Gavrikov, K. E., Nilson, J. E., Dmitriev, A. V., Zucker, C. L., & Mangel, S. C. (2006). Dendritic compartmentalization of chloride cotransporters underlies directional responses of starburst amacrine cells in retina. *Proc Natl Acad Sci U S A, 103*(49), 18793-18798. doi:10.1073/pnas.0604551103

Graveley, B. R., Brooks, A. N., Carlson, J. W., Duff, M. O., Landolin, J. M., Yang, L., . . . Celniker, S. E. (2011). The developmental transcriptome of Drosophila melanogaster. *Nature, 471*(7339), 473-479. doi:10.1038/nature09715

Grueber, W. B., Jan, L. Y., & Jan, Y. N. (2002). Tiling of the Drosophila epidermis by multidendritic sensory neurons. *Development, 129*(12), 2867-2878.

Han, C., Wang, D., Soba, P., Zhu, S., Lin, X., Jan, L. Y., & Jan, Y. N. (2012). Integrins regulate repulsion-mediated dendritic patterning of drosophila sensory neurons by restricting dendrites in a 2D space. *Neuron, 73*(1), 64-78. doi:10.1016/j.neuron.2011.10.036

Hergovich, A., Bichsel, S. J., & Hemmings, B. A. (2005). Human NDR kinases are rapidly activated by MOB proteins through recruitment to the plasma membrane and phosphorylation. *Mol Cell Biol, 25*(18), 8259-8272. doi:10.1128/MCB.25.18.8259-8272.2005

Hock, J., & Meister, G. (2008). The Argonaute protein family. *Genome Biol, 9*(2), 210. doi:10.1186/gb-2008-9-2-210

Horton, A. C., & Ehlers, M. D. (2003). Dual modes of endoplasmic reticulum-to-Golgi transport in dendrites revealed by live-cell imaging. *J Neurosci, 23*(15), 6188-6199.

Imamura, F., & Greer, C. A. (2009). Dendritic branching of olfactory bulb mitral and tufted cells: regulation by TrkB. *PLoS One, 4*(8), e6729. doi:10.1371/journal.pone.0006729

Jack, J., & Myette, G. (1997). The genes raw and ribbon are required for proper shape of tubular epithelial tissues in Drosophila. *Genetics, 147*(1), 243-253.

Jemc, J. C., Milutinovich, A. B., Weyers, J. J., Takeda, Y., & Van Doren, M. (2012). raw Functions through JNK signaling and cadherin-based adhesion to regulate Drosophila gonad morphogenesis. *Dev Biol, 367*(2), 114-125. doi:10.1016/j.ydbio.2012.04.027

Jiang, N., Soba, P., Parker, E., Kim, C. C., & Parrish, J. Z. (2014). The microRNA bantam regulates a developmental transition in epithelial cells that restricts sensory dendrite growth. *Development, 141*(13), 2657-2668. doi:10.1242/dev.107573

Jinushi-Nakao, S., Arvind, R., Amikura, R., Kinameri, E., Liu, A. W., & Moore, A. W. (2007). Knot/Collier and cut control different aspects of dendrite cytoskeleton and synergize to define final arbor shape. *Neuron, 56*(6), 963-978. doi:10.1016/j.neuron.2007.10.031

Jones, D. N., Searles, M. A., Shaw, G. L., Churchill, M. E., Ner, S. S., Keeler, J., . . . Neuhaus, D. (1994). The solution structure and dynamics of the DNA-binding domain of HMG-D from Drosophila melanogaster. *Structure, 2*(7), 609-627.

Kania, A., Salzberg, A., Bhat, M., D'Evelyn, D., He, Y., Kiss, I., & Bellen, H. J. (1995). P-element mutations affecting embryonic peripheral nervous system development in Drosophila melanogaster. *Genetics, 139*(4), 1663-1678.

Katsuki, T., Joshi, R., Ailani, D., & Hiromi, Y. (2011). Compartmentalization within neurites: its mechanisms and implications. *Dev Neurobiol, 71*(6), 458-473. doi:10.1002/dneu.20859

Kim, W. J., Jan, L. Y., & Jan, Y. N. (2012). Contribution of visual and circadian neural circuits to memory for prolonged mating induced by rivals. *Nat Neurosci, 15*(6), 876-883. doi:10.1038/nn.3104

Koike-Kumagai, M., Yasunaga, K., Morikawa, R., Kanamori, T., & Emoto, K. (2009). The target of rapamycin complex 2 controls dendritic tiling of Drosophila sensory neurons through the Tricornered kinase signalling pathway. *EMBO J, 28*(24), 3879-3892. doi:10.1038/emboj.2009.312

Lee, J., Peng, Y., Lin, W. Y., & Parrish, J. Z. (2015). Coordinate control of terminal dendrite patterning and dynamics by the membrane protein Raw. *Development, 142*(1), 162-173. doi:10.1242/dev.113423

Long, H., Ou, Y., Rao, Y., & van Meyel, D. J. (2009). Dendrite branching and self-avoidance are controlled by Turtle, a conserved IgSF protein in Drosophila. *Development, 136*(20), 3475-3484. doi:10.1242/dev.040220

Masland, R. H. (2004). Neuronal cell types. *Curr Biol, 14*(13), R497-500. doi:10.1016/j.cub.2004.06.035

Millward, T. A., Hess, D., & Hemmings, B. A. (1999). Ndr protein kinase is regulated by phosphorylation on two conserved sequence motifs. *J Biol Chem, 274*(48), 33847-33850.

Olesnicky, E. C., Killian, D. J., Garcia, E., Morton, M. C., Rathjen, A. R., Sola, I. E., & Gavis, E. R. (2014). Extensive use of RNA-binding proteins in Drosophila sensory neuron dendrite morphogenesis. *G3 (Bethesda), 4*(2), 297-306. doi:10.1534/g3.113.009795

Papoulas, O., Hays, T. S., & Sisson, J. C. (2005). The golgin Lava lamp mediates dynein-based Golgi movements during Drosophila cellularization. *Nat Cell Biol, 7*(6), 612-618. doi:10.1038/ncb1264

Rogers, S. L., & Rogers, G. C. (2008). Culture of Drosophila S2 cells and their use for RNAi-mediated loss-of-function studies and immunofluorescence microscopy. *Nat Protoc, 3*(4), 606-611. doi:10.1038/nprot.2008.18

Satoh, D., Sato, D., Tsuyama, T., Saito, M., Ohkura, H., Rolls, M. M., . . . Uemura, T. (2008). Spatial control of branching within dendritic arbors by dynein-dependent transport of Rab5-endosomes. *Nat Cell Biol, 10*(10), 1164-1171. doi:10.1038/ncb1776

Tamaskovic, R., Bichsel, S. J., Rogniaux, H., Stegert, M. R., & Hemmings, B. A. (2003). Mechanism of Ca2+-mediated regulation of NDR protein kinase through autophosphorylation and phosphorylation by an upstream kinase. *J Biol Chem, 278*(9), 6710-6718. doi:10.1074/jbc.M210590200

Tian, G., & Cowan, N. J. (2013). Tubulin-specific chaperones: components of a molecular machine that assembles the alpha/beta heterodimer. *Methods Cell Biol, 115*, 155-171. doi:10.1016/B978-0-12-407757-7.00011-6

Vo, N. K., Cambronne, X. A., & Goodman, R. H. (2010). MicroRNA pathways in neural development and plasticity. *Curr Opin Neurobiol, 20*(4), 457-465. doi:10.1016/j.conb.2010.04.002

Wiedenmann, J., Ivanchenko, S., Oswald, F., Schmitt, F., Rocker, C., Salih, A., . . . Nienhaus, G. U. (2004). EosFP, a fluorescent marker protein with UV-inducible green-to-red fluorescence conversion. *Proc Natl Acad Sci U S A, 101*(45), 15905-15910. doi:10.1073/pnas.0403668101

Ye, B., Zhang, Y., Song, W., Younger, S. H., Jan, L. Y., & Jan, Y. N. (2007). Growing dendrites and axons differ in their reliance on the secretory pathway. *Cell, 130*(4), 717-729. doi:10.1016/j.cell.2007.06.032

Yuste, R. (2013). Electrical compartmentalization in dendritic spines. *Annu Rev Neurosci, 36*, 429-449. doi:10.1146/annurev-neuro-062111-150455